nature communications

Article

https://doi.org/10.1038/s41467-025-66943-x

USP16 S-nitrosylation aggravates coronary microembolization-induced myocardial injury via repressing KDM1A-mediated glutathione homeostasis

Received: 27 September 2024

Accepted: 19 November 2025

Published online: 03 December 2025

Check for updates

Qiang Su[1,2], Jiao-Qin Qin[3], Yuan Huang[2], Ri-Xin Dai[4], Qing-Yun Wu[4], Li-Rong Mo[2] ✉, Qiang Wu[5] ✉, Wan-Zhong Huang[2] ✉, Hua-Feng Yang[6], Yang-Chun Liu[6] & Di-Guang Pan[1] ✉

Coronary microembolization (CME) is a serious cardiovascular complication that causes severe cardiac dysfunction and arrhythmias. Glutathione (GSH) exhaustion-induced oxidative stress is a key contributor to CME. Here, we explore the molecular mechanisms underlying GSH imbalance during CME. We show that CME induces myocardial injury by disturbing GSH homeostasis, which is ameliorated by glutamate-cysteine ligase modifier subunit (GCLM) or glutaminase (GLS) overexpression. Lysine-specific histone demethylase 1A (KDM1A) removes H3K9me1/2 from the promoter regions of *GCLM* and *GLS* to promote their epigenetic expression, thereby maintaining GSH homeostasis in CME. KDM1A is ubiquitinated at the K355 site during CME via inhibiting ubiquitin-specific peptidase 16 (USP16)-mediated deubiquitination. Inducible nitric oxide synthase (iNOS) facilitates S-nitrosylation (SNO) of USP16 at the C731 site, contributing to KDM1A ubiquitination and causing GSH imbalance during CME. Altogether, SNO-USP16 inhibition stabilizes the KDM1A protein to epigenetically activate GCLM and GLS, thus maintaining GSH homeostasis and relieving CME-induced myocardial injury.

Due to atherosclerotic plaque debris or percutaneous coronary intervention, coronary microembolization (CME) may result in decreased coronary flow reserve, cardiac dysfunction, and arrhythmia[1,2]. CME is an important predictor of adverse cardiovascular events and a poor prognosis[3]. Current treatment strategies for CME mainly include plaque stabilization and the administration of vasodilators, antiplatelets, and anti-inflammatory drugs[4]. A previous study reported that glutathione (GSH) imbalance occurs during CME-induced myocardial damage, and restoring GSH homeostasis could effectively ameliorate myocardial injury[5]. Thus, maintaining GSH homeostasis is crucial for relieving CME-induced myocardial injury. GSH homeostasis is regulated by a series of enzymes, including the glutamate-cysteine ligase modifier subunit (GCLM) and glutaminase (GLS). GCLM is the rate-limiting enzyme in GSH synthesis[6]. GLS promoted GSH synthesis by facilitating the conversion of glutamine to glutamate[7]. However, the detailed regulatory mechanisms underlying GSH imbalance during CME-induced myocardial damage remain largely unknown.

[1]Department of Cardiology, Guilin People's Hospital, Guilin, Guangxi, China. [2]Department of Cardiology, Jiangbin Hospital of Guangxi Zhuang Autonomous Region, Nanning, Guangxi, China. [3]Department of Neurology, Jiangbin Hospital of Guangxi Zhuang Autonomous Region, Nanning, Guangxi, China. [4]Department of Cardiology, Affiliated Hospital of Guilin Medical University, Guilin, Guangxi, China. [5]Senior Department of Cardiology, the Sixth Medical Center, Chinese PLA General Hospital, Beijing, China. [6]Cardiothoracic Surgery Intensive Care Unit, the First Affiliated Hospital of Guangxi Medical University, Nanning, Guangxi, China. ✉e-mail: 292318992@qq.com; wuqiang@jgc301.com; drwanzhong@163.com; diguangpan1028@163.com

https://doi.org/10.1038/s41467-025-66943-x

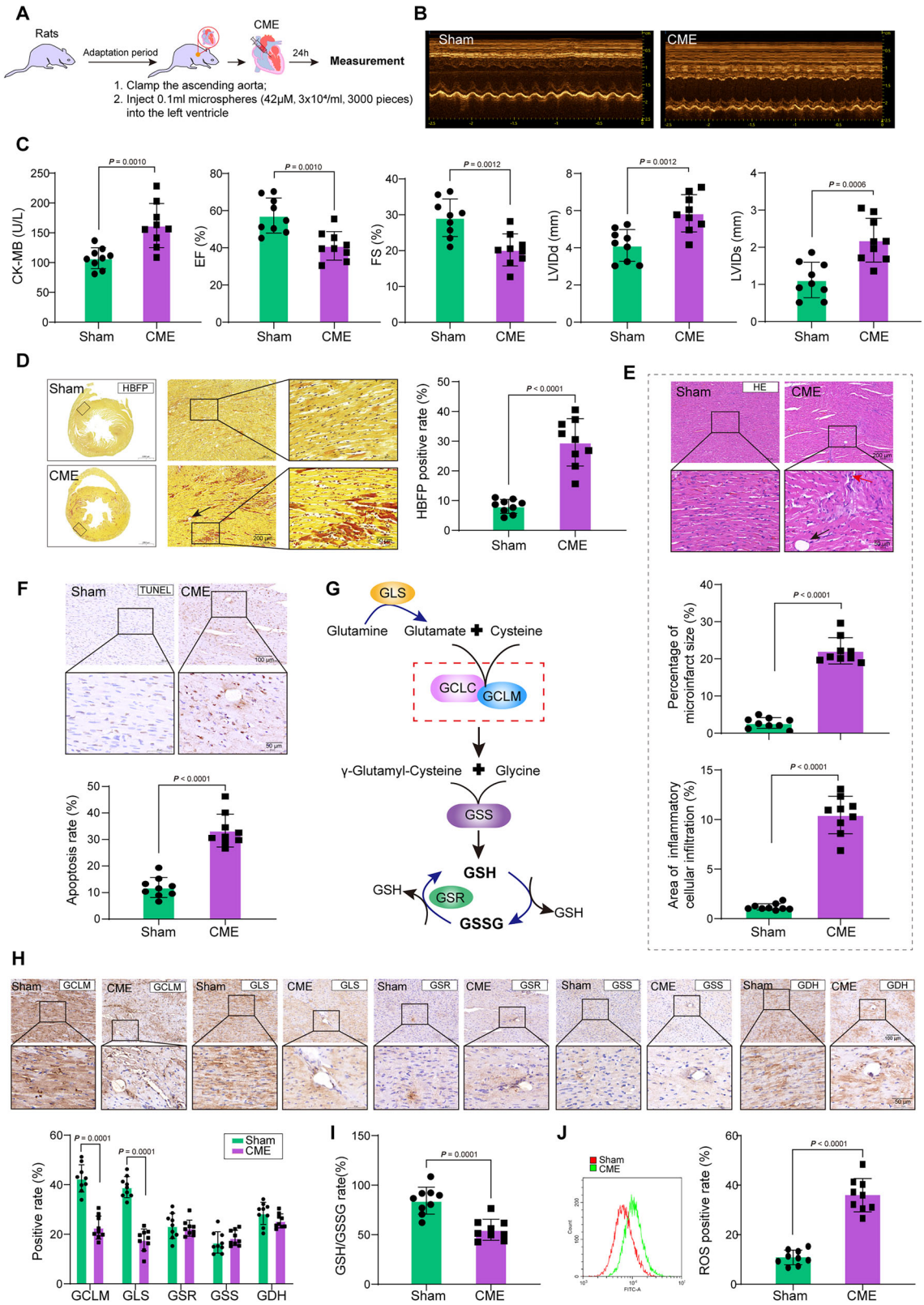

Lysine-specific histone demethylase 1A (KDM1A), also known as LSD1, is a demethylase that is required for removing the methyl marks on H3 lysine 4 (H3K4) or H3 lysine 9 (H3K9)[8]. KDM1A is involved in cardiac development[9]. He et al. reported that KDM1A protects against ischemia-reperfusion injury-induced apoptosis of cardiomyocytes via inhibiting *SOX9* transcription by reducing H3K4me3 levels at the *SOX9* promoter region[10]. In addition, KDM1A modulates histone modifications in the glutamate-cysteine ligase catalytic subunit (GCLC)-antioxidant response element region 4 (ARE4, an antioxidant regulatory element of GCLC), which restores GSH homeostasis by modulating the Nrf2-GCLC-GSH cascade in the context of diabetic retinopathy[11]. Notably, the AnimalTFDB database predicted that KDM1A might bind to the promoters of *GCLM* and *GLS*. Therefore, we speculated that KDM1A influences GSH homeostasis by regulating the transcription of *GCLM* and *GLS* during CME.

Fig. 1 | Cardiac dysfunction and GSH imbalance in CME rats. A The flowchart for the establishment of the CME model in rats. **B** Cardiac function was evaluated using echocardiography. $P = 0.0010$ for EF, $P = 0.0012$ for FS, $P = 0.0012$ for LVIDd, $P = 0.0006$ for LVIDs. **C** Serum CK-MB level was assessed using ELISA. $P = 0.0010$. **D** The myocardial microinfarct size was determined using HBFP staining (scale bar = 200 μm, 50 μm). The black arrow indicates a microsphere. $P < 0.0001$. **E** The pathological alterations in the hearts were evaluated using HE staining (scale bar = 200, 50 μm). The black arrow indicates a microsphere, and the red arrow points out aggregated inflammatory cells (leukocytes), which are manifested as inflammatory infiltration. $P < 0.0001$. **F** Apoptosis in the myocardial tissues of CME rats was observed by TUNEL (scale bar = 100, 50 μm). $P < 0.0001$. **G** The flowchart for the process of GSH synthesis. **H** The expression of GCLM, GLS, GSR, GSS, and GDH in the myocardial tissues was assessed using immunohistochemical staining (scale bar = 100, 50 μm). $P = 0.0001$ for GCLM and $P = 0.0001$ for GLS. **I** GSH and GSSG contents in heart tissues were measured to calculate the GSH/GSSG ratio. $P = 0.0001$. **J** The ROS level in frozen myocardial sections was detected by DCFH-DA staining. $P < 0.0001$. Data are presented as mean ± standard deviation (SD). $n = 9$ rats per group, indicating nine biological repetitions. In **B**, **D**–**F**, **H**, **J**, experiments were repeated independently at least 9 times with similar results. Representative images from one experiment are shown. Unpaired two-tailed Student's *t*-test (for **B**-**F**, **H**–**J**) was performed to analyze data. Source data are provided as a Source data file. GSH glutathione, CME coronary microembolization, CK-MB creatine kinase-MB, ELISA enzyme-linked immunosorbent assay, HE Hematoxylin-Eosin, TUNEL terminal deoxynucleotidyl transferase dUTP nick end labeling, GCLM glutamate-cysteine ligase modifier subunit, GLS glutaminase, GSR glutathione-disulfide reductase, GSS glutathione synthetase, GDH glutamate dehydrogenase, ROS reactive oxygen species, GSSG oxidized glutathione.

Ubiquitin-specific peptidase 16 (USP16) is a deubiquitinase that participates in the regulation of multiple biological processes such as proliferation, mitochondrial fission, and differentiation[12–14]. In addition, USP16 coordinates with the histone H2A ubiquitin ligase polycomb repressive complex 1 (PRC1) to facilitate deubiquitination of histone H2A, which consequently modulates gene transcription in hematopoietic stem cells[15]. Another study documented that USP16 deubiquitinated IKKβ to modulate the phosphorylation of p105, thereby leading to autoimmune inflammation[16]. However, the biological function of USP16 in CME remains unclear. Our preliminary mass spectrometry data showed that USP16 directly interacts with KDM1A, and in vitro experiments further demonstrated that USP16 enhances KDM1A protein levels. Whether USP16 regulates GSH homeostasis in the CME via KDM1A deubiquitination has not yet been explored.

S-nitrosylation (SNO) is a post-translational modification that contributes to the binding of nitric oxide (NO) to cysteine residues to form S-nitrosothiol[17]. SNO is involved in the pathogenesis of multiple cardiovascular disorders. For example, nitrosative stress-mediated AMPKγ-SNO could disrupt coronary collateral circulation[18]. Another study showed that inhibition of IKKγ-SNO improved cardiac function during pathological cardiac hypertrophy[19]. Notably, the GPS-SNO software predicted a potential SNO site (C731) on USP16. Our preliminary experiments confirmed that USP16 protein levels were reduced in an in vitro model of CME. Therefore, SNO-USP16 was predicted to play a role in the pathogenesis of CME.

In this study, GSH imbalance was triggered by CME and was accompanied by the downregulation of KDM1A. KDM1A overexpression restores GSH homeostasis by activating *GCLM* and *GLS* transcription. In addition, USP16 was destabilized by SNO, which consequently led to KDM1A protein degradation, leading to GSH exhaustion and aggravation of CME-induced myocardial damage. Our findings revealed a regulatory mechanism for GSH imbalance during CME, providing potential intervention targets for CME.

Results

CME disrupts cardiac function and GSH homeostasis in rats

The rat CME model was established using the flowchart shown in Fig. 1A. Echocardiographic examination revealed that the left ventricular end diastolic dimension (LVIDd), left ventricular end systolic dimension (LVIDs), left ventricular end diastolic volume (LVEDV), and left ventricular end systolic volume (LVESV) were enhanced in rats with CME, indicating that CME induced cardiac hypertrophy. In addition, left ventricular ejection fraction (EF) and ejection fraction (FS) were reduced by CME, suggesting an impairment of cardiac function (Fig. 1B, Table S1). In addition, the cardiac injury marker CK-MB was detected using ELISA, and serum CK-MB levels were strikingly elevated in CME rats (Fig. 1C). Myocardial ischemia was evaluated using HBFP staining of the left ventricle and the entire heart. The results indicated that myocardial ischemic area increased after CME, as confirmed by an increase in the percentage of HBFP-positive cells (Fig. 1D). Besides, HE staining indicated that dissolved or absent myocardial nuclei were present around the focus of microembolization, accompanied by edema and a large amount of inflammatory cell infiltration in the hearts of CME rats (Fig. 1E). TUNEL staining showed that the percentage of apoptotic cells increased in the heart after CME induction (Fig. 1F). We investigated the effects of CME on GSH homeostasis. Figure 1G illustrates the GSH synthesis process and related enzymes. Next, the differential expression of GSH synthesis-related enzymes was evaluated using immunohistochemical staining. We found lower expression of GCLM and GLS in the CME group than in the sham group, whereas GSR, GSS, and GDH expression did not differ between the CME and sham groups (Fig. 1H). Additionally, CME induction decreased the GSH/GSSG ratio and enhanced ROS levels in the myocardial tissues of rats (Fig. 1I, J), indicating that the GSH imbalance was triggered by CME. In summary, CME triggered cardiac dysfunction and GSH imbalance in vivo.

GCLM/GLS overexpression restores GSH homeostasis in the in vitro CME model

Next, hypoxia-stimulated cardiomyocytes were used to simulate CME in vitro. With the extension of hypoxia time, the GSH/GSSG ratio and cell viability were reduced, whereas ROS levels were enhanced in the cardiomyocytes (Figs. 2A, B and S1A). Consistent with the in vivo results, GCLM and GLS protein levels were reduced in a time-dependent manner by hypoxic stimulation, whereas GSS, GDH, and GSR protein levels were not affected by hypoxia (Fig. 2C). GCLM and GLS were overexpressed in H9c2 cells and primary NRVMs to further explore their influences on hypoxia-induced GSH imbalance (Fig. 2D). Functionally, overexpression of GCLM or GLS reversed the decreased GSH/GSSG ratio and cell viability and increased ROS levels upon hypoxic stimulation (Figs. 2E, F and S1B). Accordingly, the decreased GCLM and GLS protein levels induced by hypoxia were restored by GCLM and GLS overexpression, respectively (Fig. 2G). These results indicated that the hypoxia-induced GSH imbalance in cardiomyocytes was relieved by GCLM or GLS overexpression.

KDM1A overexpression attenuates CME-induced cardiac dysfunction and GSH imbalance in vivo

We focused on the demethylase KDM1A to further clarify the upstream regulatory mechanism responsible for the GSH imbalance in the CME model. Notably, we found a remarkable decrease in the expression of KDM1A in the myocardial tissues of rats with CME (Fig. 3A, Table S2), suggesting the involvement of KDM1A in CME-induced myocardial injury. AAV9-KDM1A was injected into CME rats to overexpress KDM1A to investigate the biological function of KDM1A in CME. The efficiency of KDM1A overexpression was validated using western blotting and immunohistochemical staining (Fig. S2A, B). KDM1A overexpression effectively enhanced EF and FS while reducing LVIDd, LVIDs, LVEDV, and LVESV in CME-challenged rats (Fig. 3B). Serum CK-MB levels were lower in the KDM1A overexpression group than in the CME + NC group

https://doi.org/10.1038/s41467-025-66943-x

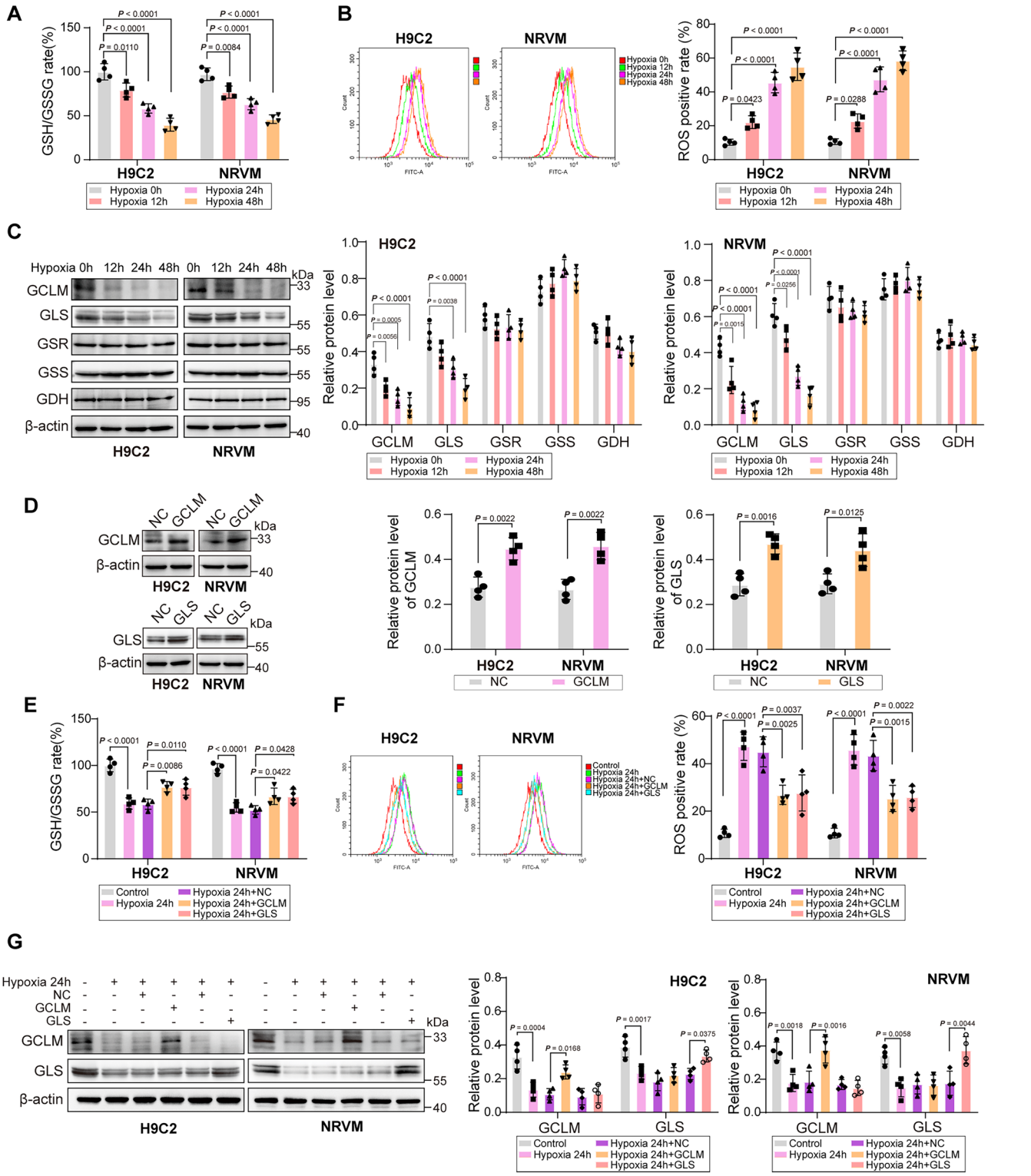

(Fig. 3C), indicating the attenuation of cardiac injury. Moreover, KDM1A overexpression reduced the percentage of HBFP-positive cells, microinfarct size, attenuated pathological changes (including edema, enlargement of myocardial cells, and inflammatory cell infiltration), and apoptosis in the myocardium of CME rats (Fig. 3D–F). Furthermore, the decreased protein levels of KDM1A, GCLM, and GLS in CME-stimulated hearts were reversed by AAV9-KDM1A injection (Figs. 3G and S2C). In addition, KDM1A overexpression partially reversed the CME-induced decrease in the GSH/GSSG ratio and elevation in ROS levels (Fig. 3H, I). These results revealed that KDM1A overexpression ameliorated CME-induced myocardial damage by restoring GSH homeostasis.

GSH imbalance in cardiomyocytes triggered by CME is alleviated by KDM1A overexpression

We further validated whether KDM1A overexpression maintains GSH homeostasis in hypoxia-stimulated cardiomyocytes in vitro. We found that hypoxia led to a time-dependent decrease in KDM1A protein levels in cardiomyocytes (Fig. 4A). Notably, GCLM and GLS protein levels were enhanced in cardiomyocytes following KDM1A overexpression

Fig. 2 | GCLM/GLS overexpression maintains GSH homeostasis in hypoxia-challenged cardiomyocytes. A The GSH/GSSG ratio in cardiomyocytes exposed to hypoxia for 12, 24, and 48 h was measured. Detailed *P* values see (**A**). **B** ROS level in cardiomyocytes after stimulation with hypoxia for 12, 24, and 48 h was detected using DCFH-DA staining. Detailed *P* values see (**B**). **C** The protein levels of GCLM, GLS, GSR, GSS, and GDH in hypoxia-stimulated cardiomyocytes were determined using western blotting. Detailed *P* values see (**C**). **D** Overexpression efficiency of GCLM and GLS in cardiomyocytes was confirmed using western blotting. GCLM or GLS-overexpressed cardiomyocytes were subjected to hypoxia for 24 h. $P = 0.0022$ for GCLM and $P = 0.0016$ for GLS in H9c2 cells, and $P = 0.0022$ for GCLM and $P = 0.0125$ for GLS in NRVM cells. **E** The GSH/GSSG ratio was calculated. Detailed *P* values see (**E**). **F** ROS level was measured using DCFH-DA staining. Detailed *P* values see (**F**). **G** Western blotting analysis of GCLM and GLS protein abundance. Detailed *P* values see (**G**). Data are presented as mean ± standard deviation (SD). $n = 4$ represents four independent biological repetitions, and each biological repetition contains three technological repetitions. In **B** & **F**, experiments were repeated independently at least 4 times with similar results. Representative images from one experiment are shown. Unpaired two-tailed Student's *t*-test (for **D**) and one-way ANOVA followed by Tukey's test for multiple group comparison (for **A**–**C**, **E**–**G**) were used to analyze data. Source data are provided as a Source data file. GCLM glutamate-cysteine ligase modifier subunit, GLS glutaminase, GSR glutathione-disulfide reductase, GSS glutathione synthetase, GDH glutamate dehydrogenase, GSH glutathione, GSSG oxidized glutathione, ROS reactive oxygen species.

(Fig. 4B). Additionally, the reduced GSH/GSSG ratio and cell viability and increased ROS levels in hypoxia-stimulated cardiomyocytes were partly counteracted by KDM1A overexpression (Figs. 4C, D and S1C). Moreover, decreased protein levels of KDM1A, GCLM, and GLS in hypoxia-stimulated cardiomyocytes were reversed by KDM1A overexpression (Fig. 4E). Thus, KDM1A overexpression was responsible for GSH homeostasis in the in vitro model of CME.

KDM1A promotes transcription and expression of GCLM and GLS in cardiomyocytes

KDM1A was knocked down in H9c2 cells and NRVMs to explore the effect of KDM1A on GSH-related protein expression. Only the mRNA and protein levels of GCLM and GLS were distinctly reduced in cardiomyocytes after KDM1A knockdown (Figs. 5A and S3A, B). Furthermore, the Animal TFDB database was used to predict the potential binding sites (BS) of KDM1A to *GCLM* and *GLS* promoters. Figure 5B illustrates that KDM1A possesses three BS to *GCLM* or *GLS* promoters (BS1, BS2, and BS3), and the binding confidence of BS3 was lower than that of BS1-2 based on the confidence score. The ChIP assay demonstrated that KDM1A could directly bind to *GCLM* promoter (both BS1 and BS2) and KDM1A could bind to *GLS* promoter (only BS2), with BS3 and IgG as negative controls (Fig. 5C). However, binding of KDM1A to *GCLM* and *GLS* promoters was weakened when KDM1A was silenced (Fig. 5D). Moreover, the ChIP-re-ChIP assay indicated that the removal of H3K9me1/2 from *GCLM* and *GLS* promoters was restrained by KDM1A depletion in cardiomyocytes, using IgG as a negative control (Fig. S4A). Collectively, KDM1A directly binds to *GCLM* and *GLS* promoters to enhance their transcription and expression.

USP16 deubiquitinates KDM1A in the in vitro CME model

Given that KDM1A protein expression was reduced in CME, we further investigated its exact mechanism. Protein degradation can be achieved through the ubiquitin-proteasome system and autophagy. Hypoxia-stimulated cardiomyocytes were treated with either MG132 (a proteasome inhibitor) or chloroquine (CQ, an autophagy inhibitor) to investigate the mechanism underlying KDM1A protein degradation. We found that the hypoxia-induced downregulation of KDM1A was partly reversed by MG132 rather than by CQ, suggesting that KDM1A was degraded via the ubiquitin-proteasome system but not via autophagy (Fig. 6A). In addition, the Co-IP assay showed that the ubiquitin level of KDM1A increased in hypoxia-challenged cardiomyocytes in a time-dependent manner (Fig. 6B). Consistently, the ubiquitin level of the KDM1A protein was enhanced in the myocardial tissues of CME rats (Fig. 6C). E3 ubiquitin ligases are ubiquitination-catalyzing enzymes that play key roles in the ubiquitin-proteasome system[20]. Mass spectrometry was performed to screen for potential E3 ubiquitin ligases and deubiquitinases of KDM1A. Based on the results of mass spectrometry, USP16 (deubiquitinase) and RNF138 (E3 ubiquitin ligase) were the candidates screened by overlapping the data (Fig. 6D). Additionally, USP16 protein levels in cardiomyocytes were reduced by hypoxia in a time-dependent manner, whereas RNF138 protein levels were not affected by hypoxia (Fig. 6E). Moreover, the KDM1A protein levels were reduced by USP16 knockdown and slightly enhanced by RNF138 knockdown (Fig. 6F). Notably, the Co-IP assay validated the exogenous and endogenous interactions between KDM1A and USP16/RNF138 proteins (Fig. 6G). Here, exogenous refers to the exogenous expression of KDM1A and USP16/RNF138 in 293T cells, and endogenous refers to the endogenous expression of KDM1A and USP16/RNF138 in cardiomyocytes. Under normal conditions, USP16 deficiency strengthened the interplay between the E3 ubiquitin ligase RNF138 and KDM1A, thereby facilitating the ubiquitination and degradation of the KDM1A protein in cardiomyocytes (Fig. S5A, B). However, RNF138 silencing enhanced the binding of USP16 to KDM1A in cardiomyocytes (Fig. S5C). KDM1A protein levels were enhanced by RNF138 silencing via inhibition of ubiquitination under hypoxic conditions (Fig. S5D). Under normal conditions, KDM1A tended to bind to USP16 but not to RNF138, which was reversed under hypoxic conditions (Fig. S5E). Therefore, the degradation of the KDM1A protein is caused by RNF138-mediated ubiquitination upon hypoxic stimulation. Furthermore, MG132 treatment partially reversed shUSP16-mediated KDM1A protein degradation (Fig. S5F). Cycloheximide (CHX) is an inhibitor of protein synthesis that facilitates protein degradation via the lysosomal system. Therefore, the CHX chase assay is widely used to evaluate protein degradation[21]. Our results indicated that KDM1A protein degradation upon CHX exposure was accelerated in USP16-depleted cardiomyocytes (Fig. S5G). Taken together, the inhibition of USP16-mediated deubiquitination led to low expression of the KDM1A protein in hypoxia-exposed cardiomyocytes.

KDM1A is ubiquitinated at the K355 site under hypoxic conditions

To further identify the specific ubiquitination site on the KDM1A protein, the K355 site was screened by mass spectrometry analysis (Fig. 7A). In this study, the peptide segment (QK355CPLYEANGQADTVK) was identified using mass spectrometry. Therefore, K355 is the ubiquitination site for KDM1A. Subsequently, we investigated whether KDM1A is ubiquitinated at K355. H9c2 cells were transfected with KDM1A-WT or KDM1A-K355R together with HA-ubiquitin. Co-IP assays revealed that the ubiquitin level of KDM1A was lower in the KDM1A-K355R group than in the KDM1A-WT group under hypoxic conditions (Fig. 7B). In addition, USP16 knockdown enhanced the ubiquitin level of KDM1A in the KDM1A-WT group of hypoxia-stimulated H9c2 cells, which were abolished in the KDM1A-K355R group (Fig. 7C). Moreover, the K355 site mutation enhanced the GSH/GSSG ratio and cell viability but reduced ROS levels in H9c2 cells (Figs. 7D, E and S1D). USP16 depletion reduced the GSH/GSSG ratio and cell viability and increased ROS levels in KDM1A-WT-transfected H9c2 cells, whereas these changes were abolished by the K355 site mutation (Figs. 7D, E and S1D). Furthermore, USP16 knockdown reduced the protein levels of KDM1A, GCLM, and GLS in the KDM1A-WT group of hypoxia-exposed H9c2 cells but did not affect that of the KDM1A-K355R group (Fig. 7F). These results proved that USP16 restrained the ubiquitination of KDM1A protein at the K355.

https://doi.org/10.1038/s41467-025-66943-x

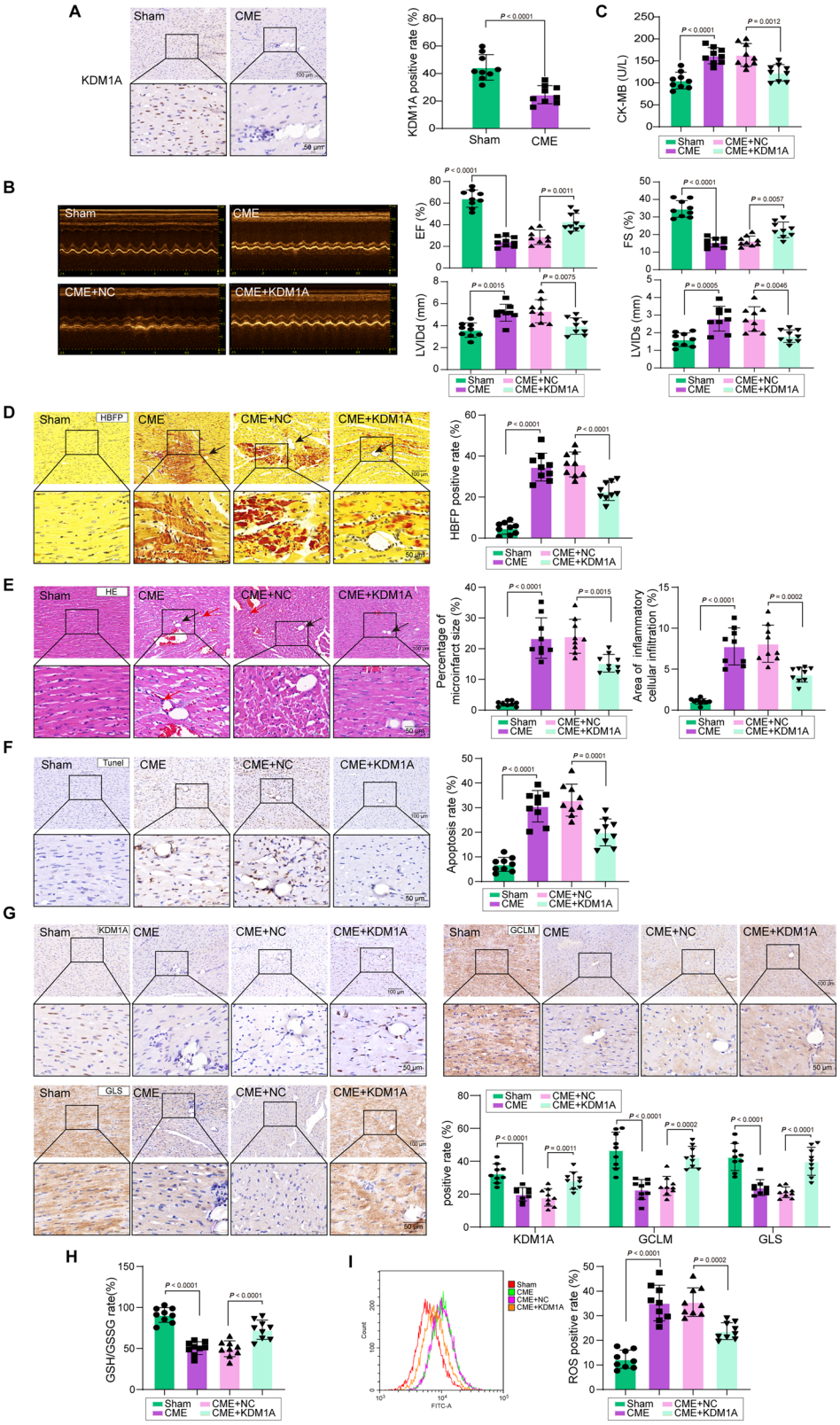

Inhibition of SNO-USP16 at the C731 site improves GSH homeostasis in CME models

SNOs are redox-based protein modifications that regulate the biological function of various enzymes[22]. Therefore, we measured SNO-USP16 levels using a biotin-switch assay. As shown in Fig. S6A, SNO-USP16 levels in the myocardial tissues of CME rats were markedly higher than those in sham rats. Consistently, SNO-USP16 levels were elevated in hypoxia-challenged cardiomyocytes (Fig. S6B). Furthermore, the GPS-SNO database predicted that USP16 might be S-nitrosylated at the C731 site, which is highly conserved among humans, mice, and rats (Fig. 8A). Additionally, hypoxia led to elevated SNO-USP16 levels in USP16-WT-transfected cardiomyocytes, which were abrogated by the C731 mutation (Fig. 8B). In addition, the decreased GSH/GSSG ratio and cell viability and enhanced ROS levels

Fig. 3 | KDM1A overexpression improves cardiac dysfunction and GSH imbalance in CME rats in vivo. A KDM1A expression in myocardial tissues was evaluated using immunohistochemical staining (scale bar = 100, 50 μm). $P < 0.0001$. **B** Cardiac function was determined using echocardiography. Detailed *P* values see (**B**). **C** Serum CK-MB level was measured using ELISA. Detailed *P* values see (**C**). **D** HBFP staining analyzed the microinfarct size in the hearts (scale bar = 100, 50 μm). The black arrow indicates a microsphere. Detailed *P* values see (**D**). **E** The pathological alterations in the myocardial tissues were observed by HE staining (scale bar = 100, 50 μm). The black arrow indicates a microsphere, and the red arrow indicates inflammatory cell infiltration. Detailed *P* values see (**E**). **F** Apoptosis in the myocardial tissues was assessed using TUNEL (scale bar = 100, 50 μm). Detailed *P* values see (**F**). **G** The expression of KDM1A, GCLM, and GLS in the myocardial tissues was measured using immunohistochemical staining (scale bar = 100, 50 μm). Detailed *P* values see (**G**). **H** The GSH/GSSG ratio in the heart tissues was calculated. Detailed *P* values see (**H**). **I** DCFH-DA staining detected the ROS level in the myocardial sections. Detailed *P* values see (**I**). Data are presented as mean ± standard deviation (SD). $n = 9$ rats per group, indicating nine biological repetitions. In **A**, **B**, **D**–**G**, **I**, experiments were repeated independently at least 9 times with similar results. Representative images from one experiment are shown. Unpaired two-tailed Student's *t*-test (for **A**) and one-way ANOVA followed by Tukey's test for multiple group comparison (for **B**–**I**) were performed to analyze data. Source data are provided as a Source data file. KDM1A lysine-specific histone demethylase 1A, GSH glutathione, CME coronary microembolization, CK-MB creatine kinase-MB, ELISA enzyme-linked immunosorbent assay, HE Hematoxylin-Eosin, TUNEL terminal deoxynucleotidyl transferase dUTP nick end labeling, GCLM glutamate-cysteine ligase modifier subunit, GLS glutaminase, GSSG oxidized glutathione, ROS reactive oxygen species.

in hypoxia-stimulated cardiomyocytes were reversed by the C731 mutation (Figs. 8C, D and S1E). Moreover, USP16-WT transfection downregulated KDM1A, GCLM, and GLS protein levels under hypoxic conditions, which were partially counteracted in USP16-C731A-transfected cardiomyocytes (Fig. 8E). Next, we validated the role of SNO-USP16 in CME in vivo. Delivery of AAV9-USP16-WT or AAV9-USP16-C731A significantly increased USP16 protein levels in rat heart tissues (Fig. S7A). In addition, the decreased USP16 protein levels in the hearts of CME rats were enhanced by AAV9-USP16-WT or AAV9-USP16-C731A (Fig. S7B). Moreover, the enhanced SNO-USP16 levels in the CME model were lowered by infection with AAV9-USP16-WT, which was more apparent in the AAV9-USP16-C731A infection group (Fig. S7C). Furthermore, AAV9-USP16-WT delivery effectively improved cardiac function in CME rats, as confirmed by enhanced levels of EF and FS, and reduced serum CK-MB, LVIDd, LVIDs, LVEDV, and LVESV, and these changes were augmented by AAV9-USP16-C731A delivery (Fig. 9A, B, Table S3). Histopathological examinations indicated that overexpression of WT-USP16 relieved ischemia, microembolization, and apoptosis in the hearts of CME rats, which intensified after C731 site mutation (Fig. 9C–E). In addition, the CME-mediated downregulation of USP16, KDM1A, GCLM, and GLS expression was recovered by USP16-WT overexpression, and this change was strengthened by USP16-C731A overexpression (Figs. 9F and S7B). In addition, the GSH/GSSG ratio was higher, and the ROS level was lower in the USP16-WT group than in the CME group, which was more pronounced in the USP16-C731A group (Fig. S8A, B). These findings suggest that SNO-USP16 at the C731 site is involved in CME-induced GSH imbalance.

SNO-USP16 at the C731 site facilitates KDM1A ubiquitination

Given that SNO-USP16 contributed to GSH imbalance during CME, we further elucidated whether SNO-USP16 could affect KDM1A protein ubiquitination. Co-IP assays revealed that the interplay between USP16 and KDM1A proteins was attenuated under hypoxic conditions, which could be restored by mutation at the C731 site (Fig. 10A, Table S4). Notably, KDM1A protein levels were upregulated by USP16-C731A transfection or MG132 treatment in hypoxia-exposed cardiomyocytes, which was further strengthened by the combination of USP16-C731A transfection and MG132 treatment (Fig. 10B). Moreover, the CHX chase assay indicated that the degradation of the KDM1A protein in hypoxia-stimulated cardiomyocytes was delayed by USP16-C731A transfection (Fig. 10C). The ubiquitination level of KDM1A was elevated by hypoxic stimulation, which was abolished in USP16-C731A-transfected cardiomyocytes (Fig. 10D). Thus, inhibition of SNO-USP16 at the C731 site suppresses the ubiquitination and degradation of KDM1A.

iNOS-mediated SNO-USP16 contributes to CME-induced GSH imbalance and KDM1A downregulation

NO production is promoted by iNOS activation upon hypoxia stimulation[23]. Excessive NO production can facilitate SNO of proteins in the pathogenesis of diverse disorders[24]. Therefore, we further explored the regulation of iNOS by SNO-USP16 in the context of CME. 1400 W is a selective inhibitor of iNOS widely used in the in vitro and in vivo experiments[25,26]. As shown in Fig. S9A, treatment with the iNOS inhibitor 1400 W effectively reversed the hypoxia-induced upregulation of SNO-USP16. Furthermore, the interaction between USP16 and KDM1A was weakened under hypoxic conditions and was restored by 1400 W (Fig. S9B). Hypoxia-induced decreases in the GSH/GSSG ratio, cell viability, and elevated ROS levels were partly counteracted by 1400 W (Figs. S9C, D and S1F). Moreover, 1400 W treatment partially reversed the decreased protein levels of USP16, KDM1A, GCLM, and GLS in hypoxia-stimulated cardiomyocytes (Fig. S9E). We evaluated the effects of iNOS inhibition on CME in vivo. 1400 W administration improved cardiac function in CME rats, as evidenced by enhanced EF and FS levels and decreased serum CK-MB, LVIDd, LVIDs, LVEDV, and LVESV levels (Fig. S10A, B, Table S4). In addition, 1400 W treatment reduced the ischemic area and inhibited apoptosis and microembolization in the hearts of CME rats (Fig. S10C–E). Subsequently, the increased expression of iNOS and decreased expression of USP16, KDM1A, GCLM, and GLS in the heart tissues of CME rats were abolished by 1400 W treatment (Fig. S10F). The enhanced SNO-USP16 levels in the CME group were partially reduced by 1400 W irradiation (Fig. S10G). Additionally, 1400 W treatment increased the GSH/GSSG ratio and reduced ROS levels in the hearts of CME rats (Fig. S10H, I). Taken together, iNOS facilitated SNO-USP16 to impair GSH homeostasis in the CME by reducing KDM1A expression.

Discussion

CME is a spontaneous event during myocardial ischemia-reperfusion injury and is a critical complication of percutaneous coronary intervention[27]. It has been reported that inhibition of oxidative stress may ameliorate CME-induced myocardial injury, suggesting that oxidative stress was a crucial driver for CME[28]. As a key antioxidant, GSH is pivotal in protecting against oxidative stress injury[29]. Consistent with previous studies, our data showed that CME resulted in GSH imbalance. GSH synthesis can be controlled by a series of enzymes, including GCLM, GLS, GSR, GSS, and GDH[30]. This study found that GCLM and GLS protein levels were strikingly reduced by CME and that the overexpression of GCLM or GLS protected against CME-induced myocardial injury. Therefore, restoring GCLM- or GLS-mediated GSH homeostasis is an effective strategy for alleviating CME-induced myocardial injury.

Methylation plays a fundamental role in ischemic myocardial injury via epigenetic regulation of target genes[31]. As a demethylase, KDM1A removes the methyl groups from methylated H3K4 and H3K9[32]. We further validated that KDM1A was abnormally downregulated in CME models and that restoring KDM1A expression attenuated CME-induced cardiac injury by maintaining GSH homeostasis. A previous study demonstrated that KDM1A epigenetically regulates TIMP1 expression by removing methylated H3K4me2 from the TIMP1

https://doi.org/10.1038/s41467-025-66943-x

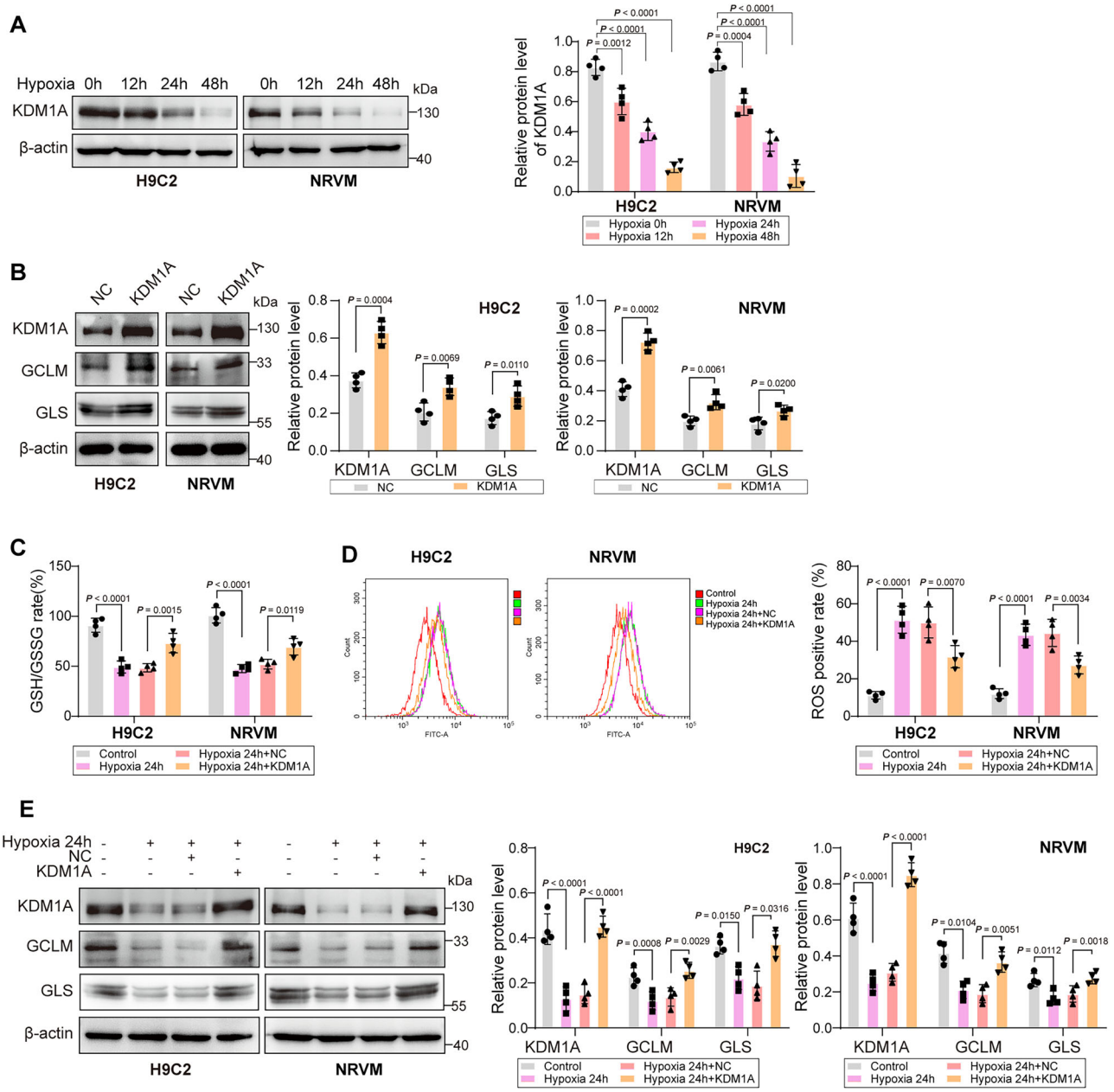

Fig. 4 | KDM1A overexpression alleviates CME-induced GSH imbalance in cardiomyocytes. A KDM1A expression in cardiomyocytes stimulated with hypoxia for 12, 24, and 48 h was assessed using western blotting. Detailed *P* values see (**A**). **B** Western blotting analysis of KDM1A, GCLM, and GLS protein levels in cardiomyocytes after KDM1A overexpression. KDM1A-overexpressed cardiomyocytes were stimulated with hypoxia for 24 h. $P = 0.0004$ for KDM1A, $P = 0.0069$ for GCLM, and $P = 0.0110$ for GLS in H9c2 cells, and $P = 0.0002$ for KDM1A, $P = 0.0061$ for GCLM, and $P = 0.0200$ for GLS in NRVM cells. **C** The GSH/GSSG ratio was calculated. Detailed *P* values see (**C**). **D** ROS production was assessed using DCFH-DA staining. Detailed *P* values see (**D**). **E** Western blotting analysis of KDM1A, GCLM, and GLS protein levels. Detailed *P* values see (**E**). Data are presented as mean ± standard deviation (SD). $n = 4$ represents four independent biological repetitions, and each biological repetition contains three technological repetitions. In **A**, **B**, **D**, **E**, experiments were repeated independently at least 4 times with similar results. Representative images from one experiment are shown. Unpaired two-tailed Student's *t*-test (for **B**) and one-way ANOVA followed by Tukey's test for multiple group comparison (for **A**, **C**–**E**) were used to analyze data. Source data are provided as a Source data file. KDM1A lysine-specific histone demethylase 1A, GSH glutathione, CME coronary microembolization, GCLM glutamate-cysteine ligase modifier subunit, GLS glutaminase, GSSG oxidized glutathione, ROS reactive oxygen species.

promoter, contributing to papillary thyroid cancer progression[33]. Another study showed that KDM1A facilitates TLR4 transcription and expression by inhibiting the methylation of H3K9 at the *TLR4* promoter, thereby aggravating renal inflammation[34]. In line with these previous findings, we demonstrated that KDM1A directly binds to *GCLM* and *GLS* promoter regions to promote their expression via the removal of H3K9me1/2. Our results provide the evidence that KDM1A triggers *GCLM* and *GLS* transcription and expression through the demethylation of H3K9me1/2 to maintain GSH homeostasis and consequently relieve CME-induced cardiac injury.

We focused on protein degradation, ubiquitination, and autophagy to further elucidate the upstream regulatory mechanisms of KDM1A in CME. Our data indicated that inhibition of ubiquitination, but not autophagy, restored KDM1A protein expression in the CME

https://doi.org/10.1038/s41467-025-66943-x

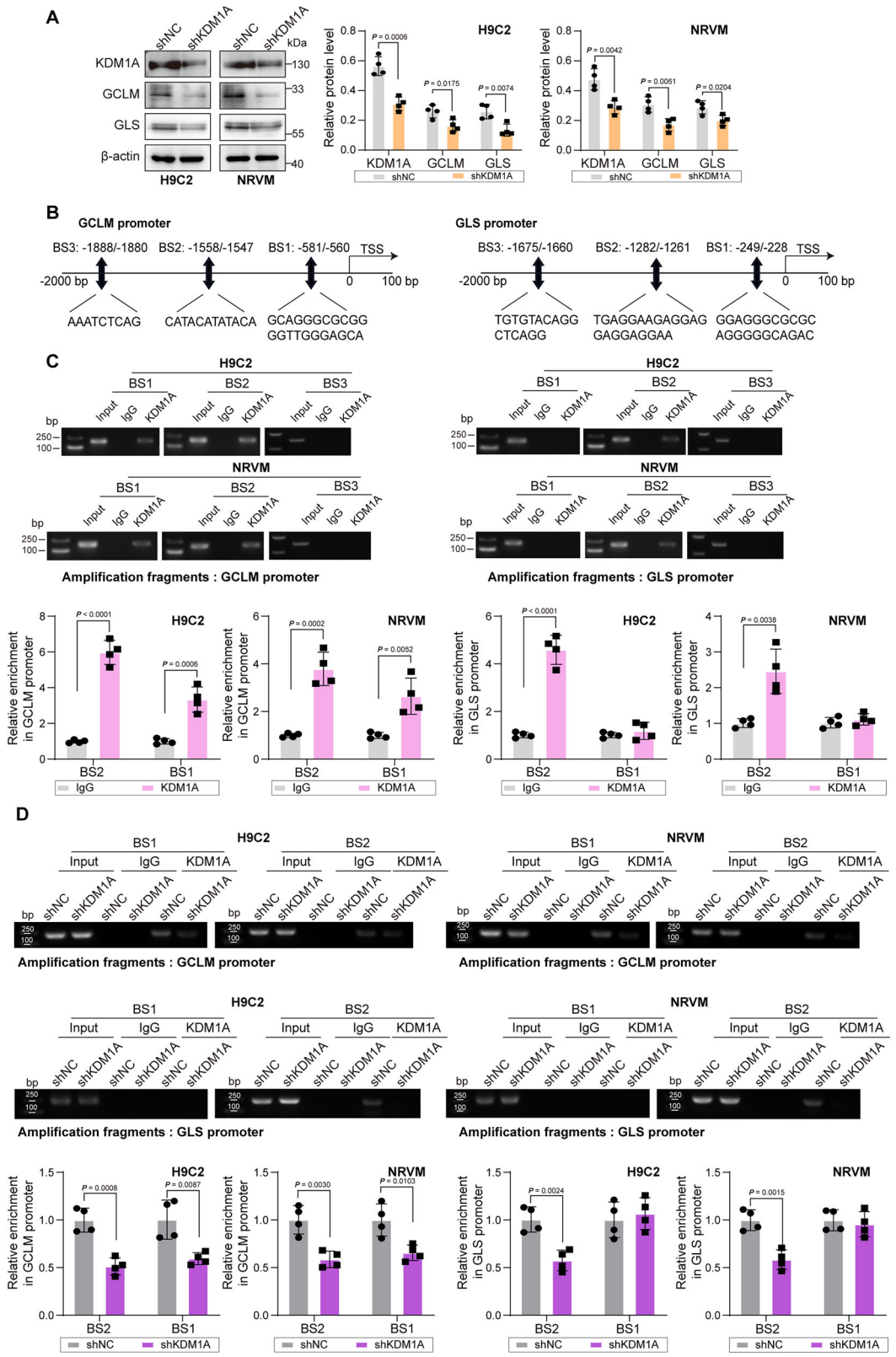

model. Thus, CME may decrease KDM1A protein expression via ubiquitination. Protein ubiquitination is a reverse process dynamically regulated by E3 ligases and deubiquitinases[35]. Mass spectrometry analysis revealed that both the E3 ligase RNF138 and deubiquitinase USP16 may modulate the KDM1A protein in the CME model. USP16-mediated deubiquitination of KEAP1 participates in hepatic ischemia-reperfusion injury[36]. Another study showed that the E3 ligase RNF138 contributes to the degradation of target proteins via ubiquitination[37]. In this study, hypoxia inhibited USP16-mediated deubiquitination but promoted RNF138-mediated ubiquitination of KDM1A at the K355 site, thus leading to KDM1A protein degradation in CME.

SNO is a key post-translational modification that plays a role in the pathogenesis of various diseases, including ischemic myocardial injury[38]. Mounting evidence indicates that SNO may affect cardiac

Fig. 5 | KDM1A facilitates transcriptional activation of GCLM and GLS. **A** Western blotting analysis of KDM1A, GCLM, and GLS protein levels in shKDM1A-transfected cardiomyocytes. $P = 0.0006$ for KDM1A, $P = 0.0175$ for GCLM, and $P = 0.0074$ for GLS in H9c2 cells, and $P = 0.0042$ for KDM1A, $P = 0.0061$ for GCLM. and $P = 0.0204$ for GLS in NRVM cells. **B** AnimalTFDB database predicted the binding sites of KDM1A to *GCLM* and *GLS* promoters. **C** The interplay between KDM1A to *GCLM* and *GLS* promoters was verified using ChIP. $P < 0.0001$ for BS2 in *GCLM* promoter, $P = 0.0006$ for BS1 in *GCLM* promoter from H9c2 cells, and $P = 0.0002$ for BS2 in *GCLM* promoter, $P = 0.0052$ for BS1 in *GCLM* promoter from NRVM cells; $P < 0.0001$ for BS2 in *GLS* promoter from H9c2 cells and $P = 0.0038$ for BS2 in *GLS* promoter from NRVM cells. **D** The binding of KDM1A to *GCLM* and *GLS* promoters in shKDM1A-transfected cardiomyocytes was evaluated using ChIP. $P = 0.0008$ for BS2 in *GCLM* promoter, $P = 0.0087$ for BS1 in *GCLM* promoter from H9c2 cells, and $P = 0.0030$ for BS2 in *GCLM* promoter, $P = 0.0103$ for BS1 in *GCLM* promoter from NRVM cells; $P = 0.0024$ for BS2 in *GLS* promoter from H9c2 cells and $P = 0.0015$ for BS2 in *GLS* promoter from NRVM cells. Data are presented as mean ± standard deviation (SD). $n = 4$ represents four independent biological repetitions, and each biological repetition contains three technological repetitions. In **A**, **C**, **D**, experiments were repeated independently at least 4 times with similar results. Representative images from one experiment are shown. Unpaired two-tailed Student's *t*-test (for **A**, **C**, **D**) was performed to analyze data. Source data are provided as a Source data file. KDM1A lysine-specific histone demethylase 1A, GCLM glutamate-cysteine ligase modifier subunit, GLS glutaminase, ChIP chromatin immunoprecipitation.

function under both physiological and pathological conditions by regulating oxidative stress[39,40] SNO-USP16 levels were markedly increased by CME treatment in this study. A previous study showed that SNO modification of PDH and KGDH proteins serves as a feedback inhibitor for H_2O_2 production in response to GSH oxidation[41], suggesting that SNO regulates GSH homeostasis. This study demonstrates the contribution of SNO-USP16 to GSH imbalance in CME. Furthermore, inhibition of SNO-USP16 at the C731 site restrained the overproduction of ROS and restored GSH homeostasis, thus mitigating CME-induced myocardial injury.

Given that USP16 can deubiquitinate KDM1A, we further evaluated the effect of SNO-USP16 on KDM1A ubiquitination. In this study, hypoxia-induced ubiquitination and degradation of the KDM1A protein were abolished by mutation of SNO-USP16 at C731. Therefore, SNO-USP16 could facilitate the ubiquitination and degradation of KDM1A in CME. NO is a major molecule that promotes SNO modification of proteins, and iNOS can trigger NO production[42]. Moreover, abnormally high iNOS expression has been found in various cardiovascular disorders, such as heart failure and myocardial ischemia[43,44]. Guo et al. documented that iNOS triggers mitochondrial dysfunction in heart failure by inducing SNO-Akt at the C224 site[45]. In the present study, we provide evidence that iNOS contributes to SNO-USP16 at the C731 site and subsequently results in KDM1A protein ubiquitination, thus leading to a GSH imbalance under hypoxic conditions. These findings prove that iNOS-mediated SNO-USP16 promotes CME progression.

This study had some limitations. First, our data were not validated in gene-knockout animals or clinical samples. Second, there is a lack of in vitro models of CME. To some extent, we used a hypoxia-challenged cell model to mimic CME, which may not reflect all aspects of CME. Third, KDM1A has been reported to control gene expression by regulating miRNA[46]. Further investigations are required to determine whether KDM1A controls GSH-related gene expression by regulating miRNAs. Fourth, rats are the small animal most commonly used to establish CME models via nonselective coronary vascular embolization. Owing to the limitations of the experimental conditions, the current research is unable to determine the exact location of the microembolization could not be determined, which is a drawback of this study. Fifth, we used 42-μm microspheres that can block blood vessels of the corresponding diameter. The hearts of small animals are small in volume, and conventional imaging techniques (such as ultrasound and magnetic resonance imaging) have insufficient resolution to identify embolized cardiac vessels. Therefore, we could not detect the specific microvascular embolization positions in rats with CME.

In conclusion, our results confirmed that iNOS-mediated SNO-USP16 served as a driver of ubiquitination and degradation of KDM1A protein, which disrupted GSH homeostasis and exacerbated CME-induced myocardial injury (Fig. S11). Our findings provide insights into the regulatory mechanisms underlying GSH homeostasis that protect cells from CME-induced myocardial injury.

Methods

Animal model

Three-month-old male Sprague-Dawley rats (weighing approximately 300 g) were purchased from the Hunan SLAC Laboratory Animal Center (Changsha, China). After a 2-week adaptation period under standard feeding conditions, CME was induced in rats as previously described[47]. Briefly, the rats were intraperitoneally injected with 40 mg/kg pentobarbital hydrochloride for anesthesia, followed by ventilation using a small-animal ventilator. The ascending aorta was exposed via thoracotomy. After clamping for 10 s, the microspheres (3000 spheres of 42 μm in 100 μL normal saline, Cat. no: 07314-5; Polysciences, Warrington, PA, USA) was injected into the left ventricle of each rat using a microsyringe, while the sham rats were injected with 100 μL normal saline. The thoracic cavity was closed, and the skin was sutured. The rats were intraperitoneally injected with 1400 W (5 mg/kg) to inhibit inducible nitric oxide synthase (iNOS). Serum and heart samples were collected 24 h after CME induction. This study was approved by the Ethics Committee of the Jiangbin Hospital of Guangxi Zhuang Autonomous Region (Certificate No. KY-GZR2024-003) and the Laboratory Animal Ethics Committee of Guilin Medical University (Certificate No. GLMC20243332), and the Animal Care and Welfare Committee of Guangxi Medical University (Certificate No. 202408025).

Adeno-associated virus serotype 9 (AAV9) delivery in rats

According to previous studies, AAV9 exhibits distinct preferential effects in the heart[48,49]. To evaluate the biological functions of KDM1A and SNO-USP16, AAV9-GFP, AAV9-KDM1A, AAV9-USP16-WT, AAV9-USP16-C731A (the SNO site at C731 was mutated to alanine), and the CMV promoter were produced by Fenghbio Co., Ltd. (Changsha, China). The rats were injected with AAV9 (10^{11} TU in 200 μL in vivo transfection reagents) via the tail veins 3 weeks before CME induction.

Cardiac function evaluation

For cardiac function evaluation, the parameters of EF, FS, LVIDd, LVIDs, LVEDV, and LVESV were detected using echocardiography on the echography device (Sonos7500 Series; Philips, Cambridge, MA, USA) with the probe frequency at 12 MHz. Stroke volume (SV) = LVEDV − LVESV. EF = SV/LVEDV × 100%. The operator was blinded to the grouping assignment, and all values were averaged over three cardiac cycles. All analyzed parameters are presented in Supplementary Tables 1–4.

Detection of serum creatine kinase-MB (CK-MB) level

Serum CK-MB levels were assessed using an ELISA kit (SEA479Ra; USCN, Wuhan, China) following the manufacturer's protocol.

Histopathological examination

The rat hearts were fixed with 4% paraformaldehyde, embedded in paraffin and cut into 4-μm sections. Pathological changes in the heart tissues were determined using a hematoxylin-eosin (HE) staining kit

https://doi.org/10.1038/s41467-025-66943-x

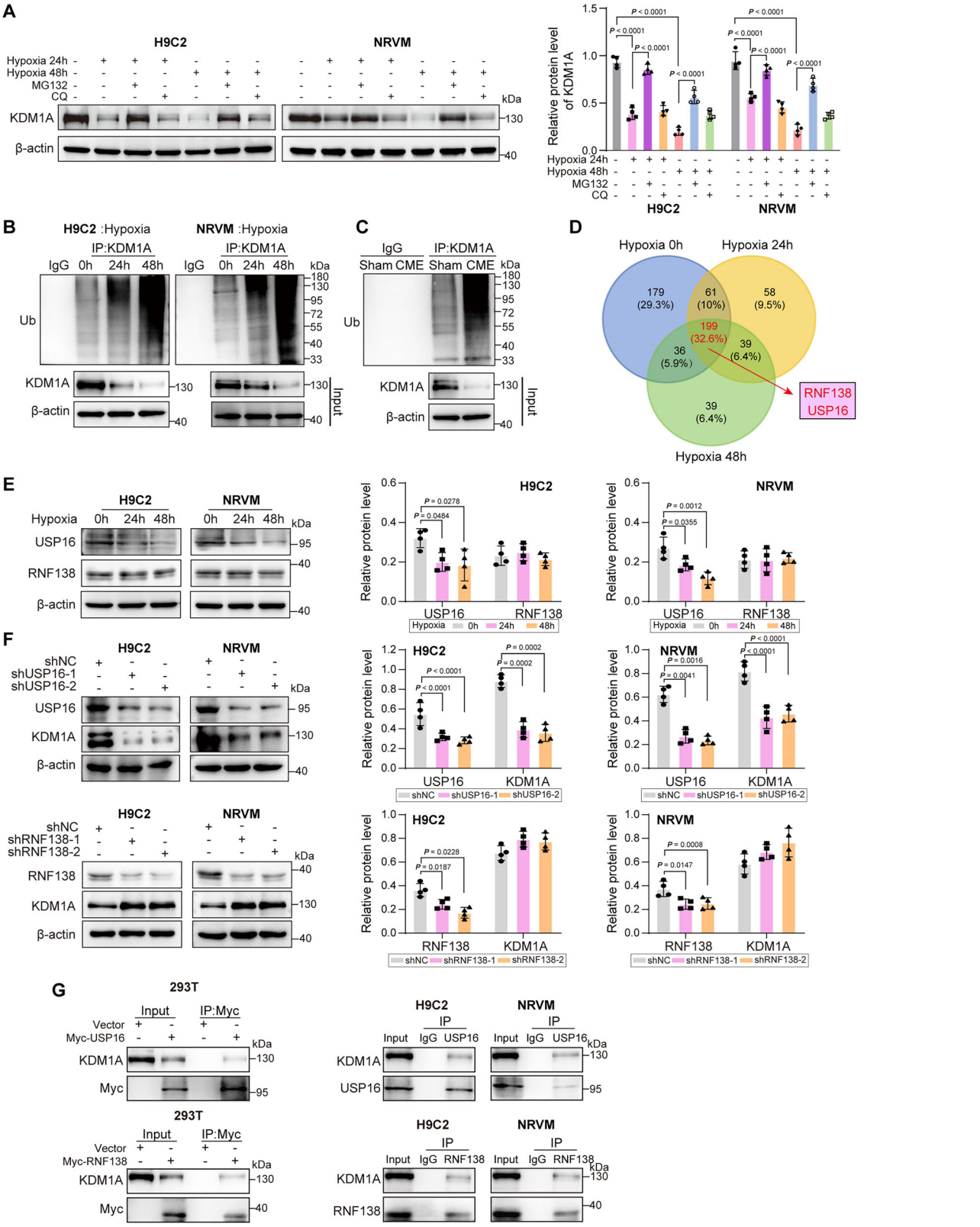

(Solarbio, Beijing, China) and observed under a microscope (Olympus, Tokyo, Japan). For each rat, an average of three sections from different areas of the heart was quantified using Image-Pro Plus 6.0 (Media Cybernetics, Rockville, MD, USA). The microinfarct size was calculated as microinfarct area/total observed area × 100%, and the degree of inflammatory cell infiltration was presented as the ratio of infiltration area to total area × 100%. Hematoxylin basic fuchsin picric acid (HBFP) staining is a sensitive method for the early diagnosis of myocardial ischemia[50]. The paraffin-embedded heart sections were subjected to HBFP staining to measure myocardial microinfarct size. Briefly, the sections were deparaffinized using xylene, counterstained using alum hematoxylin and basic fuchsin, differentiated in 0.1% picric acid acetone, and stained with aniline blue. Finally, stained sections were

Fig. 6 | USP16 stabilizes KDM1A in the in vitro CME model via deubiquitination. **A** Hypoxia-stimulated cardiomyocytes were treated with MG132 or CQ, and KDM1A protein abundance was detected using western blotting. Detailed *P* values see (**A**). **B** Co-IP analyzed the ubiquitination level of KDM1A in hypoxia-exposed cardiomyocytes. **C** The ubiquitination level of KDM1A in the heart tissues of CME rats was evaluated using Co-IP. **D** E3 ligases and deubiquitinases interacting with KDM1A were analyzed using mass spectrometry. **E** The protein abundance of USP16 and RNF138 in hypoxia-challenged cardiomyocytes was assessed using western blotting. Detailed *P* values see (**E**). **F** Western blotting analysis of KDM1A and USP16/RNF138 expression in cardiomyocytes transfected with shUSP16-1/2 or shRNF138-1/2. Detailed *P* values see (**F**). **G** The interplay between KDM1A and USP16/RNF138 was validated by Co-IP. Data are presented as mean ± standard deviation (SD). $n = 4$ represents four independent biological repetitions, and each biological repetition contains three technological repetitions. In **A**–**C**, **E**–**G**, experiments were repeated independently at least 4 times with similar results. Representative images from one experiment are shown. One-way ANOVA followed by Tukey's test for multiple group comparison (for **A**, **E**, **F**) was used to analyze data. Source data are provided as a Source data file. USP16 ubiquitin-specific peptidase 16, KDM1A lysine-specific histone demethylase 1A, CME coronary microembolization, MG132 Z-Leu-Leu-Leu-al, CQ chloroquine, Co-IP Co-immunoprecipitation, RNF138 ring finger protein 138.

examined under a light microscope. Positive HBFP staining indicated heart ischemia.

Terminal deoxynucleotidyl transferase dUTP nick end labeling (TUNEL)

The TUNEL assay was used to analyze apoptosis using a commercial TUNEL Assay Kit (ab206386, Abcam, Cambridge, UK) according to the manufacturer's instructions. In short, the paraffin-embedded sections were rehydrated with gradient ethanol, permeabilized with Proteinase K, treated with 30% H_2O_2, incubated with the TdT Labeling Reaction Mix for 1.5 h, and developed using the diaminobenzidine (DAB) solution. Finally, positive TUNEL staining was examined under a light microscope.

Immunohistochemical staining

Heart sections were subjected to antigen retrieval using Trilogy solution (Sigma-Aldrich, St. Louis, MO, USA). Endogenous peroxidase was blocked using 15% hydrogen peroxide, followed by incubation with 10% goat serum. The sections were incubated with primary antibodies against GCLM (catalog number: AFRM9359, clone name: AFKL9359, 1:50, Aifang Biological, Changsha, China), GLS (catalog number: AFRM80717, clone name: AFKL80717, 1:50; Aifang Biological), GSR (catalog number: PA5-29945, 1:100; Invitrogen, Waltham, MA, USA), GSS (catalog number: bs-11850R, 1:100; Bioss Inc., Woburn, MA, USA), GDH (catalog number: ab170895, clone name: EPR12338(B), 1:100; Abcam), KDM1A (catalog number: #2139, 1:50; Cell Signaling Technology, Danvers, MA, USA) overnight at 4 °C, followed by incubation with a secondary antibody (catalog number: bs-0293M, 1:200; Bioss Inc.). Sections were developed using a diaminobenzidine (DAB) solution and observed under a light microscope.

Cell culture and treatment

H9c2 cardiomyocytes were purchased from the American Type Culture Collection (CRL-1446; American Type Culture Collection, Manassas, VA, USA) and cultured with Dulbecco's modified Eagle medium (DMEM, Sigma-Aldrich) containing 10% fetal bovine serum (Sigma-Aldrich) with 5% CO_2 at 37 °C. Primary neonatal rat ventricular myocytes (NRVMs) were isolated from 1-day-old male neonatal Sprague-Dawley rats (Hunan SLAC Laboratory Animal Center). Briefly, the hearts were isolated from neonatal rats after cervical dislocation. NRVMs were extracted using a Pierce Cardiomyocyte Isolation Kit (cat. 88281; Thermo Fisher Scientific, Waltham, MA, USA), according to the manufacturer's protocol. The isolated NRVMs were cultured with DMEM containing 10% fetal bovine serum with 5% CO_2 at 37 °C, with culture medium changed every 2 days. All cells tested negative for mycoplasma contamination.

H9c2 cells and primary NRVMs were maintained in serum-free DMEM and exposed to hypoxic conditions (1% O_2/5% CO_2) for 12, 24, or 48 h to simulate the hypoxic microenvironment during CME in vitro. Control cells were cultured under normal conditions (21% O_2/5% CO_2). The inducible nitric oxide synthase (iNOS) inhibitor 1400 W (100 μM, MedChem Express, Monmouth Junction, NJ, USA) was added to cardiomyocytes 15 min before hypoxia to inactivate iNOS.

Cell transfection or lentivirus infection

Short hairpin RNA (shRNA) targeting KDM1A (shKDM1A), shUSP16, shRNF138, and scrambled shRNA (shNC); single guide RNA (sgRNA) targeting USP16 (sgUSP16) and sg-NC; and overexpression plasmids for GCLM, GLS, KDM1A-WT, KDM1A-K355R (ubiquitination site at K355 was mutated), USP16-WT, USP16-C731A (SNO site at C731 was mutated), and HA-Ubiquitin were obtained from Fenghbio Co., Ltd. All sequences for shRNAs and sgRNAs are provided in Supplementary Table 5. Lentiviruses carrying GCLM, GLS, KDM1A, NC, shKDM1A, shUSP16, shRNF138, shNC, sgUSP16, and sgNC were purchased from Fenghbio Co., Ltd. H9c2 cells were planted into 6-well plates (4×10^5 per well) and transfected with the overexpression plasmids for GCLM, GLS, KDM1A-WT, KDM1A-K355R, USP16-WT, USP16-C731A, HA-Ubiquitin, sgRNAs, or shRNAs using Lipofectamine 2000 (Thermo Fisher) for 48 h. For lentivirus infection, 10^6 primary NRVMs were infected with the packaged lentiviruses with a multiplicity of infection of 50 supplemented with 4 μg/mL Polybrene.

Western blotting

Protein samples were extracted using radioimmunoprecipitation assay buffer (Solarbio, Beijing, China) containing PMSF. After detection of protein concentration using the BCA Protein Assay kit (Solarbio), 30 μg of protein samples were subjected to SDS-PAGE and transferred to the polyvinylidene fluoride membranes. The membranes were blocked with 5% skimmed milk, and incubated with primary antibodies against GCLM (catalog number: ab126704, clone name: EPR6667, 1:1000; Abcam), GLS (catalog number: ab170895, clone name: EPR12338(B), 1:1000; Abcam), GSR (catalog number: PA5-29945, 1:500; Invitrogen), GSS (catalog number: ab124811, clone name: EPR6562, 1:1000; Abcam), GDH (catalog number: ab156876, clone name: EP7212, 1:1000; Abcam), KDM1A (catalog number: ab129195, clone name: EPR6825, 1:1000, Abcam and #2139, 1:1000; CST), USP16 (catalog number: A301-614A-T, 1:1000; Invitrogen), RNF138 (catalog number: A302-993A-T, 1:500; Invitrogen), Ubiquitin (catalog. number: 13-1600, 1:500; Invitrogen), Myc (catalog number: ab32, clone name: 9E10, 1:1000; Abcam), and β-actin (catalog number: ab8226, clone name: mAbcam 8226, 1:5000; Abcam) at 4 °C overnight. After washing with TBST, the membranes were incubated with an HRP-coupled secondary antibody (catalog number: bs-0295G-HRP, 1:10000; Bioss Inc.) and visualized using ECL Substrate (Solarbio). The uncropped and unprocessed scans of all blots and gels, including all quantified replicates, are provided in "Source Data".

Reverse transcription-quantitative PCR (RT-qPCR)

Total RNA was extracted from cardiomyocytes using TRIzol reagent (Yeasen Biotechnology, Shanghai, China) and reverse-transcribed into cDNA using a First Strand cDNA Synthesis kit (Takara, Shiga, Japan). Subsequently, qPCR was performed using the SYBR Green Master Mix (Takara). Relative mRNA levels normalized to GAPDH were calculated using the $2^{-\Delta\Delta Ct}$ method. The primer sequences are listed in Supplementary Table 6.

https://doi.org/10.1038/s41467-025-66943-x

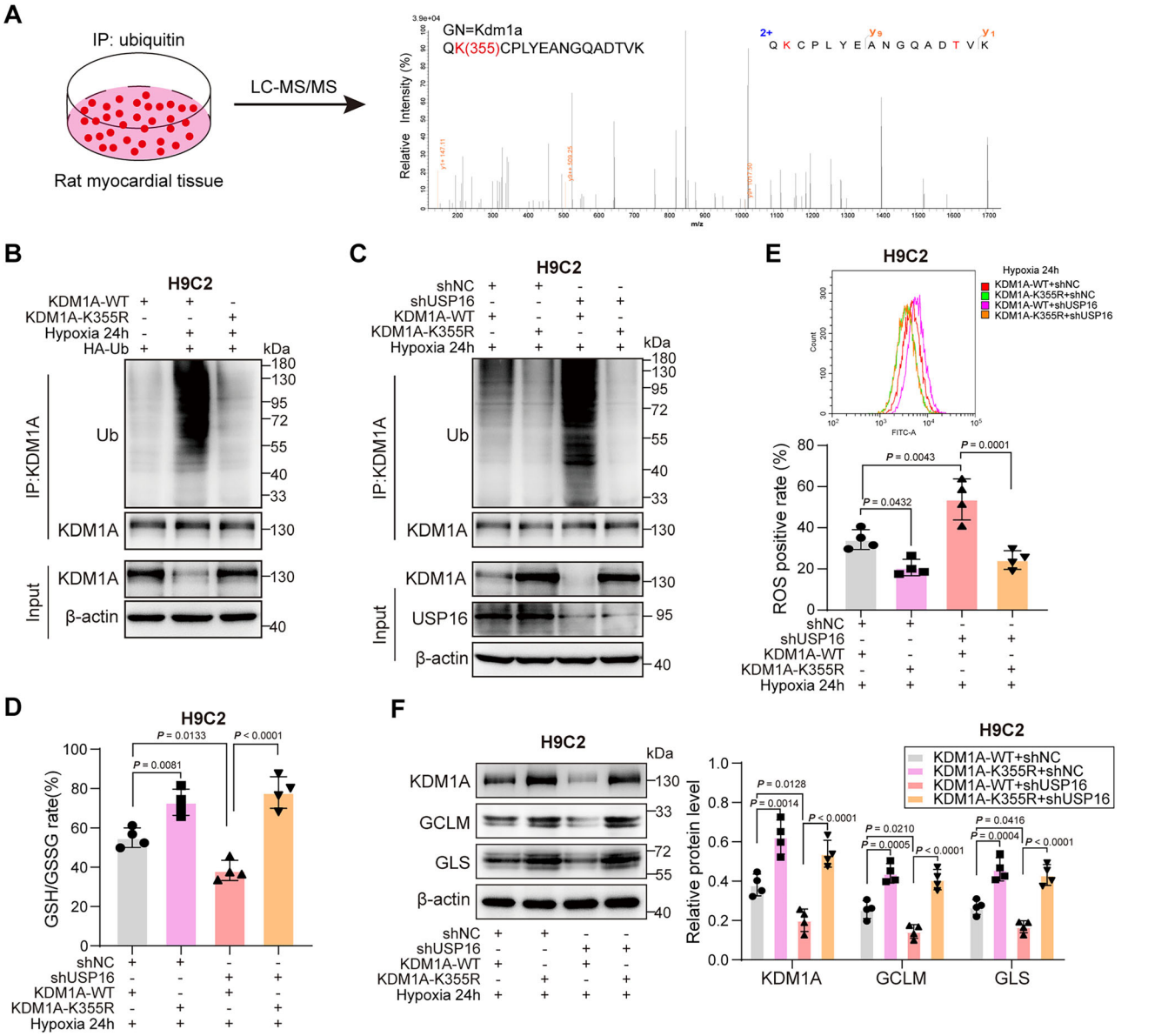

Fig. 7 | KDM1A is ubiquitinated at the K355 site in hypoxia-exposed cardiomyocytes. A The potential ubiquitination sites for KDM1A were determined using mass spectrometry. **B** H9c2 cells were transfected with KDM1A-WT or KDM1A-K355R and then subjected to hypoxia for 24 h in the presence of MG132. Co-IP analyzed KDM1A ubiquitination level. H9c2 cells were transfected with KDM1A-WT or KDM1A-K355R together with shNC or shUSP16, followed by hypoxia for 24 h. **C** KDM1A ubiquitination level was evaluated using Co-IP. **D** The GSH/GSSG ratio was calculated. Detailed *P* values see (**D**). **E** ROS production was analyzed using DCFH-DA staining. Detailed *P* values see (**E**). **F** Western blotting analysis of KDM1A, GCLM, and GLS protein levels. Detailed *P* values see (**F**). Data are presented as mean ± standard deviation (SD). $n = 4$ represents four independent biological repetitions, and each biological repetition contains three technological repetitions. In **B**, **C**, **E**, **F**, experiments were repeated independently at least 4 times with similar results. Representative images from one experiment are shown. One-way ANOVA followed by Tukey's test for multiple group comparison (for **D**–**F**) was performed to analyze data. Source data are provided as a Source data file. KDM1A lysine-specific histone demethylase 1A, MG132 Z-Leu-Leu-Leu-al, Co-IP Co-immunoprecipitation, GSH glutathione, GCLM glutamate-cysteine ligase modifier subunit, GLS glutaminase, GSSG oxidized glutathione, ROS reactive oxygen species.

Cell counting kit-8 (CCK-8)

Cardiomyocytes were seeded in 96-well plates at a density of 1×10^3 cells/well. After different treatments, the cells in each well were added with 10 μL CCK-8 reagent (Yeasen Biotechnology). After culture for 2 h at 37 °C, the absorbances were detected at a wavelength of 450 nm on a microplate reader (Thermo Fisher).

Detection of reduced glutathione (GSH) and oxidized glutathione (GSSG)

The levels of GSH and GSSG in cardiomyocytes and heart tissues were detected using commercial GSH Content Assay Kits (BC1175, Solarbio) and GSSG Content Assay Kits (BC1185, Solarbio), respectively. The GSH/GSSG ratio was calculated.

Reactive oxygen species (ROS) assay

Intracellular ROS levels were determined using the fluorescent probe DCFH-DA. Briefly, the frozen myocardial sections, H9c2 cells, and primary NRVMs were stained with 10 μmol/L DCFH-DA solution (Beyotime, Haimen, China) for 30 min at 37 °C in the dark. Subsequently, the intracellular ROS levels were assessed using flow cytometry.

https://doi.org/10.1038/s41467-025-66943-x

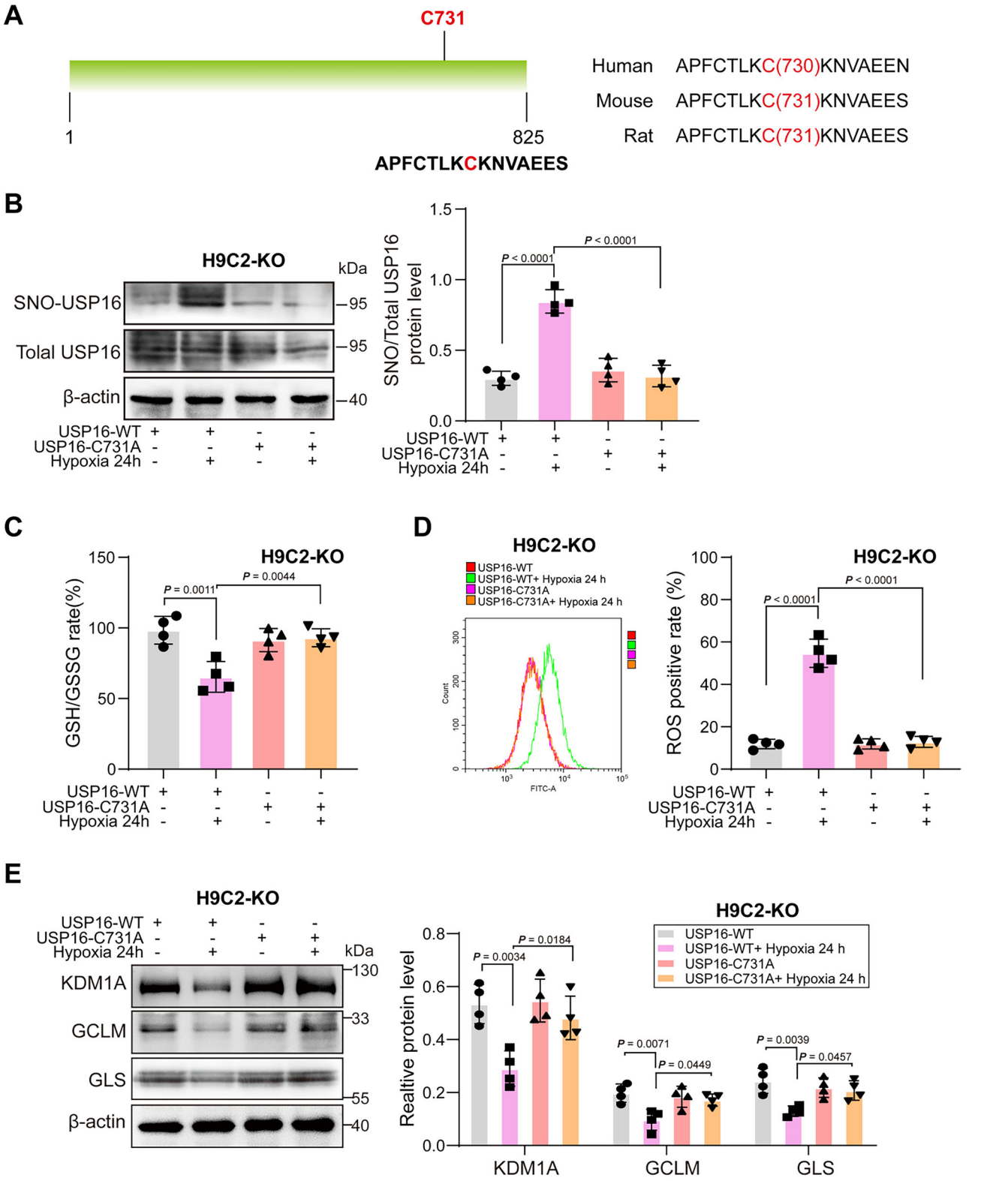

Fig. 8 | Repression of SNO-USP16 at the C731 site restores GSH homeostasis in hypoxia-stimulated cardiomyocytes. A GPS-SNO database predicted the SNO sites for USP16. H9c2-KO cells with sgUSP16 under normal or hypoxic conditions were transfected with USP16-WT or USP16-C731A. **B** Biotin-switch assay detected SNO-USP16 level in H9c2 cells. Detailed *P* values see (**B**). **C** The GSH/GSSG ratio was calculated. Detailed *P* values see (**C**). **D** ROS level was determined using DCFH-DA staining. Detailed *P* values see (**D**). **E** Western blotting analysis of KDM1A, GCLM, and GLS protein levels. Detailed *P* values see (**E**). Data are presented as mean ± standard deviation (SD). $n = 4$ represents four independent biological repetitions, and each biological repetition contains three technological repetitions. In **B**, **D**–**E**, experiments were repeated independently at least 4 times with similar results. Representative images from one experiment are shown. One-way ANOVA followed by Tukey's test for multiple group comparison (for **B**–**E**) was performed to analyze data. Source data are provided as a Source data file. SNO S-nitrosylation, USP16 ubiquitin-specific peptidase 16, GSH glutathione, GCLM glutamate-cysteine ligase modifier subunit, GLS glutaminase, GSSG oxidized glutathione, ROS reactive oxygen species.

https://doi.org/10.1038/s41467-025-66943-x

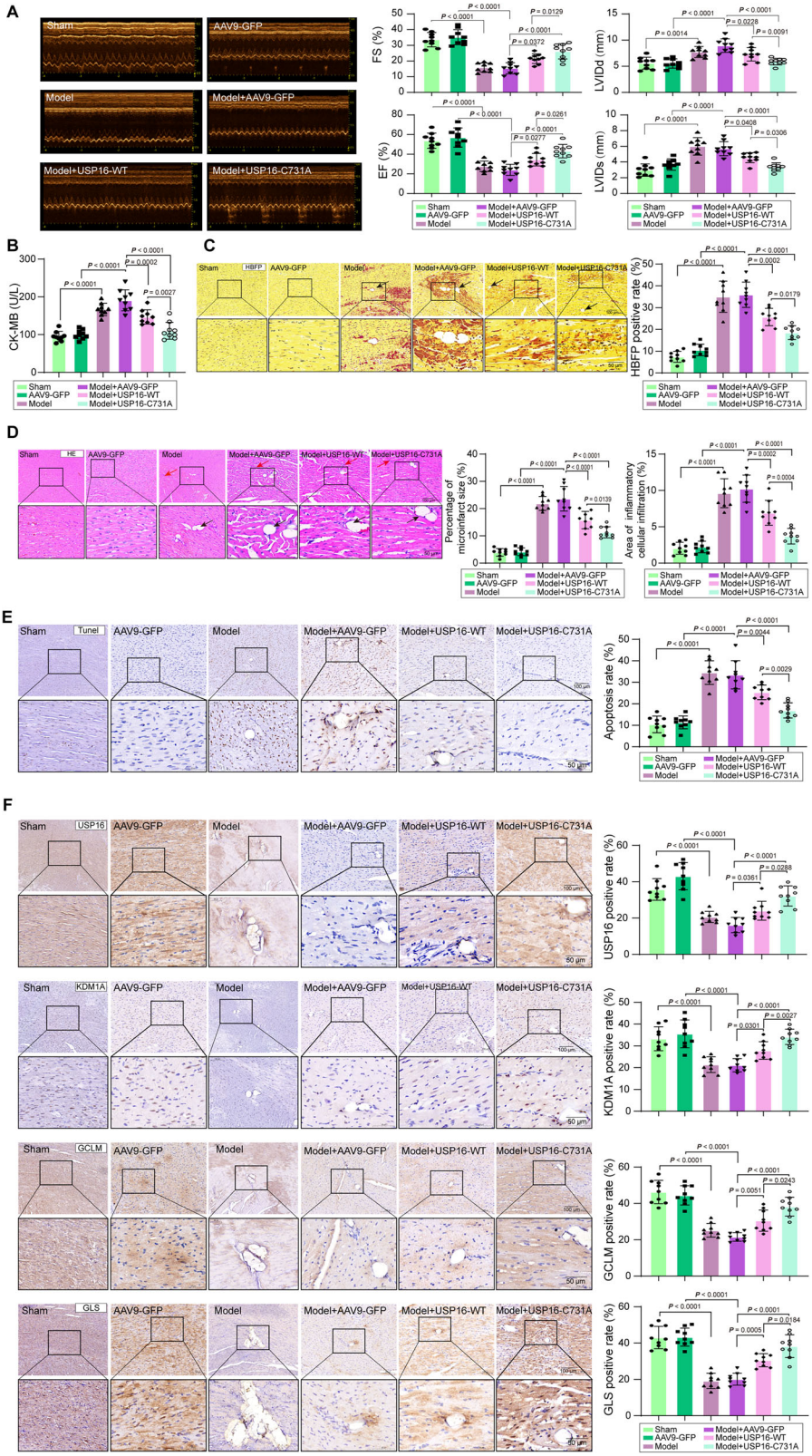

Chromatin immunoprecipitation (ChIP) and re-ChIP

For the ChIP assay, 5×10^7 cardiomyocytes (H9c2 and NRVMs isolated from approximately twenty neonatal Sprague-Dawley rats) were crosslinked with 1% formaldehyde for 10 min at room temperature and lysed using lysis buffer (0.1% SDS, 0.5% Triton X-100, and 20 mM Tris-HCl, pH 8.1). Sonication was performed on cell lysates from 5×10^7 cardiomyocytes using the 10 s on and 10 s off mode for 12 cycles at 4 °C using a Q500 sonicator (QSonica, Newtown, CT, USA) with microtip probes at 30% power. The chromatin extracts from 5×10^7 cardiomyocytes were immunoprecipitated with 2 μg of anti-KDM1A (catalog number: ab129195, clone name: EPR6825, Abcam) or 2 μg of anti-IgG (catalog number: ab172730, clone name: EPR25A, Abcam) at 4 °C overnight. Subsequently, the immunocomplexes were incubated with 50 μL of Dynabeads Protein G at 4 °C for 4 h. After de-crosslinking and

https://doi.org/10.1038/s41467-025-66943-x

Fig. 9 | Inhibition of SNO-USP16 at the C731 site improves cardiac dysfunction and GSH imbalance in CME rats. A Cardiac function was evaluated using echocardiography. Detailed *P* values see (**A**). **B** Serum CK-MB level was measured using ELISA. Detailed *P* values see (**B**). **C** HBFP staining evaluated the microinfarct size in the heart tissues (scale bar = 100, 50 μm). The black arrow indicates a microsphere. Detailed *P* values see (**C**). **D** The pathological changes in the myocardial tissues were determined using HE staining (scale bar = 100, 50 μm). The black arrow indicates a microsphere, and the red arrow indicates inflammatory cell infiltration. Detailed *P* values see (**D**). **E** Apoptosis in the myocardial tissues was measured using TUNEL (scale bar = 100, 50 μm). Detailed *P* values see (**E**). **F** The expression of USP16, KDM1A, GCLM, and GLS in the myocardial tissues was analyzed using immunohistochemical staining (scale bar = 100, 50 μm). Detailed *P* values see (**F**). Data are presented as mean ± standard deviation (SD). *n* = 9 rats per group, indicating nine biological repetitions. In **A**, **C**–**F**, experiments were repeated independently at least 9 times with similar results. Representative images from one experiment are shown. One-way ANOVA followed by Tukey's test for multiple group comparison was performed to analyze data. Source data are provided as a Source data file. SNO S-nitrosylation, USP16 ubiquitin-specific peptidase 16, GSH glutathione, CME coronary microembolization, CK-MB creatine kinase-MB, ELISA enzyme-linked immunosorbent assay, HE Hematoxylin-Eosin, TUNEL terminal deoxynucleotidyl transferase dUTP nick end labeling, KDM1A lysine-specific histone demethylase 1A, GCLM glutamate-cysteine ligase modifier subunit, GLS glutaminase, GSH glutathione.

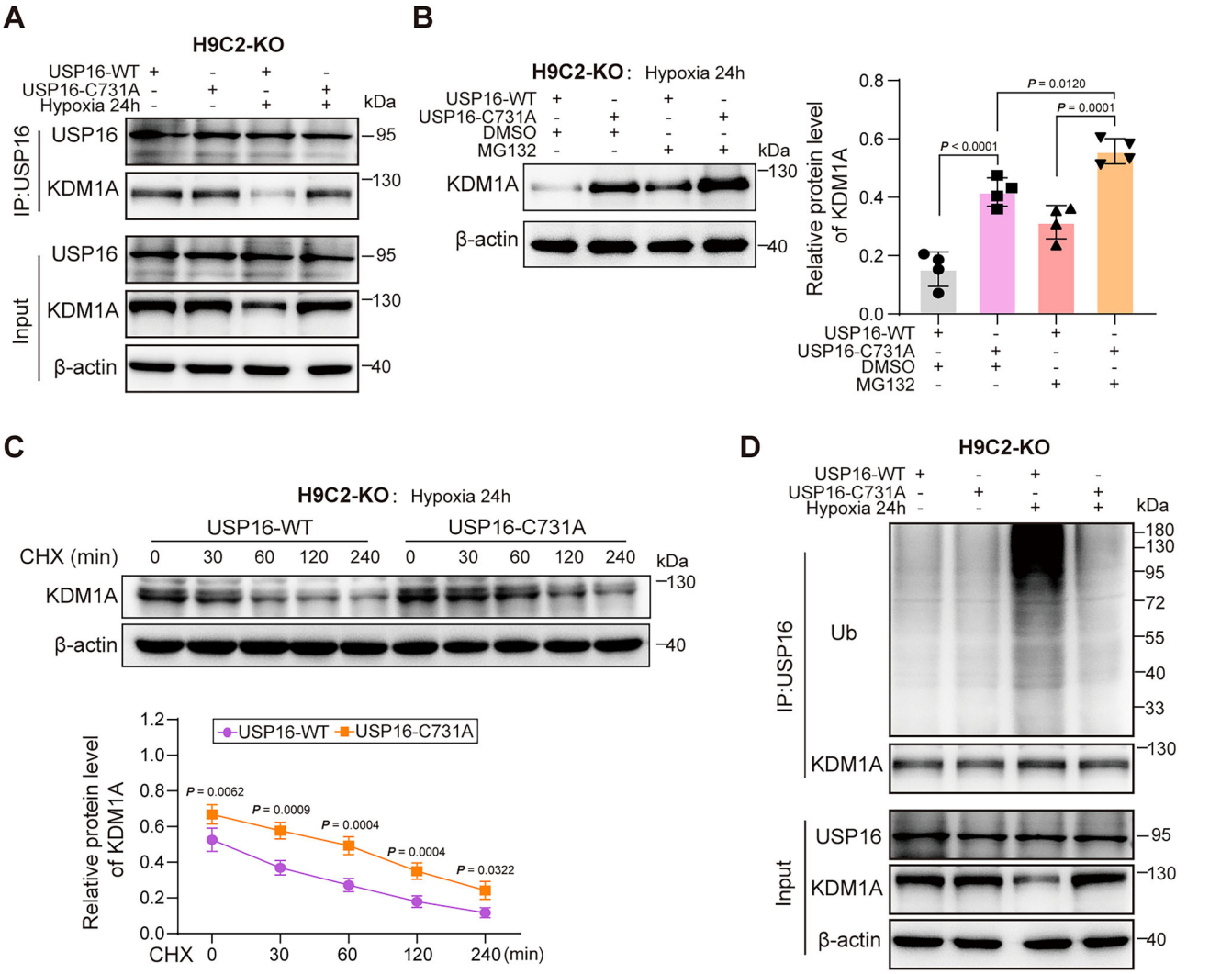

Fig. 10 | SNO-USP16 at the C731 site is responsible for hypoxia-induced KDM1A ubiquitination. H9c2-KO cells with sgUSP16 under normal or hypoxic conditions were transfected with USP16-WT or USP16-C731A. **A** Co-IP evaluated the interaction between USP16 and KDM1A proteins. **B** The protein level of KDM1A was assessed using western blotting. Detailed *P* values see (**B**). **C** The stability of KDM1A in H9c2 cells was detected using western blotting, *P* = 0.0062 for 0 min, *P* = 0.0009 for 30 min, *P* = 0.0004 for 60 min, *P* = 0.0004 for 120 min, *P* = 0.0322 for 240 min. D The ubiquitination level of KDM1A was determined using Co-IP. Data are presented as mean ± standard deviation (SD). *n* = 4 represents four independent biological repetitions, and each biological repetition contains three technological repetitions. In **A**–**D**, experiments were repeated independently at least 4 times with similar results. Representative images from one experiment are shown. One-way ANOVA followed by Tukey's test for multiple group comparison (for **B**) and unpaired two-tailed Student's *t*-test (for **C**) and were performed to analyze data. Source data are provided as a Source data file. SNO S-nitrosylation, USP16 ubiquitin-specific peptidase 16, KDM1A lysine-specific histone demethylase 1A, Co-IP Co-immunoprecipitation, sgUSP16 small guide RNA targeting USP16.

elution, enrichment of the *GCLM/GLS* promoter was evaluated using qPCR. The primer sequences are listed in Supplementary Table 7.

For re-ChIP, the immunoprecipitated DNAs by the first ChIP were subjected to a second immunoprecipitation with 2 μg of antibodies, including anti-H3K9me1 (catalog number: CSB-PA257742, 1:50, CUSABIO, Wuhan, China), anti-H3K9me2 (catalog number: CSB-PA597952, 1:50, CUSABIO), anti-H3K4me1 (catalog number: 32131, clone name: RM140, 2 μg, Cayman, MI, USA), anti-H3K4me2 (catalog number: CSB-

PA087078, 1:50, CUSABIO) or anti-IgG (catalog number: ab172730, clone name: EPR25A, Abcam). After de-crosslinking and elution, the enriched DNAs were assessed using qPCR.

Co-immunoprecipitation (Co-IP)

The exogenous interaction between USP16/RNF138 and KDM1A was validated in 293T cells. Briefly, 293T cells were transfected with Myc-USP16 or Myc-RNF138. After transfection for 24 h, the 293T cells were lysed with RIPA buffer containing protease inhibitors. Thereafter, the cell lysates were immunoprecipitated with 3 μg of anti-Myc (catalog number: AE070, clone name: ARC5004-12, ABclonal, Woburn, MA, USA) at 4 °C overnight, followed by incubation with Protein A/G Magnetic Beads for 1 h. The immunoprecipitated proteins were washed with lysis buffer, and the protein levels of Myc and KDM1A were detected by western blotting.

To evaluate endogenous protein interaction or ubiquitination level of KDM1A, the cell lysates of cardiomyocytes (H9c2 and primary NRVMs) were incubated with the protein A/G beads at 4 °C for 4 h, followed by immunoprecipitation with protein A/G-conjugated anti-KDM1A (catalog number: ab129195, clone name: EPR6825, 1:10; Abcam), anti-USP16 (catalog number: 14055-1-AP, 2 μg; Thermo Fisher), anti-RNF138 (catalog number: ABIN1931062, 2 μg; Antibodies-online, Limerick, PA, USA), anti-HA (catalog number: ab236632, clone name: EPR22819-101, 1:30; Abcam), or anti-IgG (catalog number: ab172730, clone name: EPR25A, 1:50; Abcam) at 4 °C overnight. Finally, the immunoprecipitated proteins were washed with IP lysis buffer and analyzed using western blotting.

Mass spectrometry

Cardiomyocytes (NRVMs) were infected with lentiviruses carrying the Flag-KDM1A plasmid, and cell lysates were immunoprecipitated using anti-Flag affinity magnetic beads. Immunoprecipitated proteins were subjected to protein electrophoresis, followed by Coomassie blue staining. Then the protein bands were excised and analyzed using mass spectrometry. Rat myocardial tissues were immunoprecipitated using anti-ubiquitin affinity magnetic beads. The ubiquitination sites for the KDM1A protein in the immunoprecipitates were analyzed using mass spectrometry. A mass spectrometer (Thermo Fisher Scientific) was operated in data-dependent mode (MS scans, 300–1650 m/z). Full-scan mass spectrometry spectra of the protein samples were obtained at a resolution of 60,000 at 200 m/z with a maximum injection time of 20 ms. The 15 most intense ions were fragmented using high collision-induced dissociation. The resolution was set to 15,000 at 200 m/z, AGC target to 1E5, and maximum injection time to 25 ms.

Biotin-switch assay

SNO-USP16 levels were detected using a biotin-switch assay with an S-nitrosylation Protein Detection Kit (10006518, Cayman Chemical, Ann Arbor, MI), as described by Zhao et al.[51]. Briefly, the samples were lysed and centrifuged at 500 × g for 5 min to obtain the cell pellets. Then, the cell pellets were blocked with the Blocking Reagent for 30 min at 4 °C, followed by incubation with cold acetone at −20 °C for 1 h. Thereafter, the protein pellets were incubated with the Reducing and Labeling Reagents at room temperature for 1 h. The biotin-labeled proteins were purified using the avidin-coupled agarose beads (Thermo Fisher) at 4 °C overnight. Finally, SNO-USP16 levels were measured using the USP16 antibody, as described for western blotting.

Statistical analysis

Sample size of the rats was predetermined using power analyses as described previously[52]. All experiments were conducted using at least four biological replicates, with each biological replicate containing three technical replicates. The quantitative data are displayed as mean ± standard deviation (SD). The normality of the data distribution was evaluated using the Shapiro–Wilk test. The detailed sample sizes are described in the figure legends. Statistical differences were analyzed using Student's t-test for two groups or one-way analysis of variance (ANOVA), followed by Tukey's test for multiple groups, using GraphPad Prism software (version 8.0). Statistical significance was set at $P < 0.05$.

Reporting summary

Further information on research design is available in the Nature Portfolio Reporting Summary linked to this article.

Data availability

The mass spectrometry proteomics data have been deposited to the ProteomeXchange Consortium via the PRIDE[53] partner repository with the dataset identifier PXD070144 and PXD070295. The data supporting the findings of this study are available within the Article, its Supplementary Information or Source Data file. Source data are provided with this paper.

References

1. Heusch, G. et al. Coronary microembolization: from bedside to bench and back to bedside. *Circulation* **120**, 1822–1836 (2009).
2. Skyschally, A. et al. Coronary microembolization. *Basic Res. Cardiol.* **101**, 373–382 (2006).
3. Heusch, G., Skyschally, A. & Kleinbongard, P. Coronary microembolization and microvascular dysfunction. *Int. J. Cardiol.* **258**, 17–23 (2018).
4. Kleinbongard, P. & Heusch, G. A fresh look at coronary microembolization. *Nat. Rev. Cardiol.* **19**, 265–280 (2022).
5. Liu, T. et al. Atorvastatin attenuates ferroptosis-dependent myocardial injury and inflammation following coronary microembolization via the Hif1a/Ptgs2 pathway. *Front. Pharm.* **13**, 1057583 (2022).
6. Cao, X. et al. Involvement of glutamate cysteine ligase genes in tolerance to emamectin benzoate in Spodoptera frugiperda and their putative regulatory mechanisms. *J. Agric Food Chem.* **71**, 13717–13728 (2023).
7. Tanaka, S. et al. Inhibition of glutamine metabolism increases sensitivity to plasma-activated medium-induced cytotoxicity. *Free Radic Res.* **58**, 170–179 (2024).
8. Shi, Y. et al. Histone demethylation mediated by the nuclear amine oxidase homolog LSD1. *Cell* **119**, 941–953 (2004).
9. Davis, K. et al. The role of demethylases in cardiac development and disease. *J. Mol. Cell Cardiol.* **158**, 89–100 (2021).
10. He, L., Wang, Y. & Luo, J. Epigenetic modification mechanism of histone demethylase KDM1A in regulating cardiomyocyte apoptosis after myocardial ischemia-reperfusion injury. *PeerJ* **10**, e13823 (2022).
11. Mishra, M., Zhong, Q. & Kowluru, R. A. Epigenetic modifications of Nrf2-mediated glutamate-cysteine ligase: implications for the development of diabetic retinopathy and the metabolic memory phenomenon associated with its continued progression. *Free Radic. Biol. Med* **75**, 129–139 (2014).
12. Ge, J. et al. USP16 regulates castration-resistant prostate cancer cell proliferation by deubiquitinating and stablizing c-Myc. *J. Exp. Clin. Cancer Res.* **40**, 59 (2021).
13. Wang, Q. & Qiu, H. Deubiquitinase USP16 induces gouty arthritis via Drp1-dependent mitochondrial fission and NLRP3 inflammasome activation. *Arthritis Res. Ther.* **25**, 126 (2023).
14. Yang, W. et al. The histone H2A deubiquitinase Usp16 regulates embryonic stem cell gene expression and lineage commitment. *Nat. Commun.* **5**, 3818 (2014).
15. Gu, Y. et al. The histone H2A deubiquitinase Usp16 regulates hematopoiesis and hematopoietic stem cell function. *Proc. Natl. Acad. Sci. USA* **113**, E51–E60 (2016).

16. Yu, J. S. et al. Substrate-specific recognition of IKKs mediated by USP16 facilitates autoimmune inflammation. *Sci. Adv.* **7**, eabc4009 (2021).
17. Chao, M. L. et al. S-nitrosylation-mediated coupling of G-protein alpha-2 with CXCR5 induces Hippo/YAP-dependent diabetes-accelerated atherosclerosis. *Nat. Commun.* **12**, 4452 (2021).
18. Bai, W. et al. S-nitrosylation of AMPKgamma impairs coronary collateral circulation and disrupts VSMC reprogramming. *EMBO Rep.* **25**, 128–143 (2024).
19. Datta Chaudhuri, R. et al. Cardiomyocyte-specific regression of nitrosative stress-mediated S-Nitrosylation of IKKgamma alleviates pathological cardiac hypertrophy. *Cell Signal.* **98**, 110403 (2022).
20. Qin, R. et al. Research advancements on the involvement of E3 ubiquitin ligase UBR5 in gastrointestinal cancers. *Heliyon* **10**, e30284 (2024).
21. Miao, Y. et al. Cycloheximide (CHX) chase assay to examine protein half-life. *Bio Protoc.* **13**, e4690 (2023).
22. Qi, Q. et al. Overexpression of SlMDHAR in transgenic tobacco increased salt stress tolerance involving S-nitrosylation regulation. *Plant Sci.* **299**, 110609 (2020).
23. Perez-Torres, I., Manzano-Pech, L., Rubio-Ruiz, M. E., Soto, M. E., & Guarner-Lans, V. Nitrosative stress and its association with cardiometabolic disorders. *Molecules* **25**, 2555 (2020).
24. Taniguchi, R. et al. Attenuation of protein arginine dimethylation via S-nitrosylation of protein arginine methyltransferase 1. *J. Pharm. Sci.* **154**, 209–217 (2024).
25. Cheng, X., Cheng, X. S., Kuo, K. H. & Pang, C. C. Inhibition of iNOS augments cardiovascular action of noradrenaline in streptozotocin-induced diabetes. *Cardiovasc. Res.* **64**, 298–307 (2004).
26. Xie, T. et al. GAPDH S-nitrosation contributes to age-related sarcopenia through mediating apoptosis. *Nitric Oxide* **120**, 1–8 (2022).
27. Chen, A. et al. Rosuvastatin protects against coronary microembolization-induced cardiac injury via inhibiting NLRP3 inflammasome activation. *Cell Death Dis.* **12**, 78 (2021).
28. Su, Q., Lv, X. & Ye, Z. Ligustrazine attenuates myocardial injury induced by coronary microembolization in rats by activating the PI3K/Akt pathway. *Oxid. Med. Cell Longev.* **2019**, 6791457 (2019).
29. Hu, X. et al. Brain extended and closed forms glutathione levels decrease with age and extended glutathione is associated with visuospatial memory. *Neuroimage* **293**, 120632 (2024).
30. Parsanathan, R. & Jain, S. K. Hydrogen sulfide regulates circadian-clock genes in C(2)C(12) myotubes and the muscle of high-fat-diet-fed mice. *Arch. Biochem. Biophys.* **672**, 108054 (2019).
31. Tang, Y. et al. Methylation and transcriptomic expression profiles of HUVEC in the oxygen and glucose deprivation model and its clinical implications in AMI patients. *Front. Genet.* **14**, 1293393 (2023).
32. Wojtala, M. et al. Silencing lysine-specific histone demethylase 1 (LSD1) causes increased HP1-positive chromatin, stimulation of DNA repair processes, and dysregulation of proliferation by Chk1 phosphorylation in human endothelial cells. *Cells* **8**, 1212 (2019).
33. Zhang, W. et al. Knockdown of KDM1A suppresses tumour migration and invasion by epigenetically regulating the TIMP1/MMP9 pathway in papillary thyroid cancer. *J. Cell Mol. Med.* **23**, 4933–4944 (2019).
34. Yang, Y. T., Wang, X., Zhang, Y. Y. & Yuan, W. J. The histone demethylase LSD1 promotes renal inflammation by mediating TLR4 signaling in hepatitis B virus-associated glomerulonephritis. *Cell Death Dis.* **10**, 278 (2019).
35. Dewson, G., Eichhorn, P. J. A. & Komander, D. Deubiquitinases in cancer. *Nat. Rev. Cancer* **23**, 842–862 (2023).
36. Tong, G. et al. FGF18 alleviates hepatic ischemia-reperfusion injury via the USP16-mediated KEAP1/Nrf2 signaling pathway in male mice. *Nat. Commun.* **14**, 6107 (2023).
37. Liu, W. et al. RNF138 inhibits late inflammatory gene transcription through degradation of SMARCC1 of the SWI/SNF complex. *Cell Rep.* **42**, 112097 (2023).
38. Huang, Z. M. et al. Convergence of G protein-coupled receptor and S-nitrosylation signaling determines the outcome to cardiac ischemic injury. *Sci. Signal* **6**, ra95 (2013).
39. Shi, X. & Qiu, H. Post-translational S-nitrosylation of proteins in regulating cardiac oxidative stress. *Antioxidants* **9**, 1051 (2020).
40. Fernando, V. et al. S-nitrosylation: an emerging paradigm of redox signaling. *Antioxidants* **8**, 404 (2019).
41. Chalifoux, O., Faerman, B. & Mailloux, R. J. Mitochondrial hydrogen peroxide production by pyruvate dehydrogenase and alpha-ketoglutarate dehydrogenase in oxidative eustress and oxidative distress. *J. Biol. Chem.* **299**, 105399 (2023).
42. Wang, X. et al. S-nitrosylation of NOTCH1 regulates mesenchymal stem cells differentiation into hepatocyte-like cells by inhibiting notch signalling pathway. *J. Cell Mol. Med.* **28**, e70274 (2024).
43. Zhang, P. et al. Inducible nitric oxide synthase deficiency protects the heart from systolic overload-induced ventricular hypertrophy and congestive heart failure. *Circ. Res.* **100**, 1089–1098 (2007).
44. Singh, J. et al. Amelioration of endothelial integrity by 3,5,4'-trihydroxy-trans-stilbene against high-fat-diet-induced obesity and -associated vasculopathy and myocardial infarction in rats, targeting TLR4/MyD88/NF-kappaB/iNOS signaling cascade. *Biochem. Biophys. Res. Commun.* **705**, 149756 (2024).
45. Guo, Y. et al. iNOS contributes to heart failure with preserved ejection fraction through mitochondrial dysfunction and Akt S-nitrosylation. *J. Adv. Res.* **43**, 175–186 (2023).
46. Zhao, L. J. et al. LSD1 deletion represses gastric cancer migration by upregulating a novel miR-142-5p target protein CD9. *Pharm. Res.* **159**, 104991 (2020).
47. Zhou, Y. et al. Overexpression of lncRNA TUG1 alleviates NLRP3 inflammasome-mediated cardiomyocyte pyroptosis through targeting the miR-186-5p/XIAP axis in coronary microembolization-induced myocardial damage. *Front. Immunol.* **12**, 637598 (2021).
48. Chen, B. D. et al. Targeting transgene to the heart and liver with AAV9 by different promoters. *Clin. Exp. Pharm. Physiol.* **42**, 1108–1117 (2015).
49. Liu, S. et al. Yap promotes noncanonical wnt signals from cardiomyocytes for heart regeneration. *Circ. Res.* **129**, 782–797 (2021).
50. Leadbeatter, S., Wawman, H. M. & Jasani, B. Immunocytochemical diagnosis of early myocardial ischaemic/hypoxic damage. *Forensic Sci. Int.* **40**, 171–180 (1989).
51. Zhao, S. et al. Hsp90 S-nitrosylation at Cys521, as a conformational switch, modulates cycling of Hsp90-AHA1-CDC37 chaperone machine to aggravate atherosclerosis. *Redox Biol.* **52**, 102290 (2022).
52. Zhang, Q. et al. PSD-93 interacts with SynGAP and promotes SynGAP ubiquitination and ischemic brain injury in mice. *Transl. Stroke Res.* **11**, 1137–1147 (2020).
53. Perez-Riverol, Y. et al. The PRIDE database resources in 2022: a hub for mass spectrometry-based proteomics evidences. *Nucleic Acids Res.* **50**, D543–D552 (2022).

Acknowledgements

This study was supported by the National Natural Science Foundation of China from QS (Grant No. 82260072), the National Natural Science Foundation of China from YC.L (Grant No. 82300376), and the Joint Project on Regional High-Incidence Diseases Research of Guangxi Natural Science Foundation from YC.L (Grant No.2024GXNSFBA010082).

Author contributions

Q.S. Conceptualization; experiments; writing—original draft; funding acquisition; J.Q.Q. Data curation; validation; y.h. investigation; experiments; data curation; R.X.D. Methodology; experiments; Q.Y.W. formal analysis; experiments; L.R.M. Resources; Q.W. Visualization; Project administration; W.Z.H. Writing—review and editing; H.F.Y. Data curation; experiments; Y.C.L. Visualization; funding acquisition; D.G.P. Visualization; supervision.

Competing interests
The authors declare no competing interests.

Additional information
Supplementary information The online version contains supplementary material available at https://doi.org/10.1038/s41467-025-66943-x.

Correspondence and requests for materials should be addressed to Li-Rong Mo, Qiang Wu, Wan-Zhong Huang or Di-Guang Pan.

Peer review information *Nature Communications* thanks Paul Delgado Olguin, and the other, anonymous, reviewer(s) for their contribution to the peer review of this work. A peer review file is available.